CFD in the design of gas quenching furnace

by

Olivier Macchion Faxénlaboratoriet Department of Mechanics

June 2005 Technical Reports from Royal Institute of Technology Department of Mechanics S-100 44 Stockholm, Sweden

Typsatt i $\mathcal{A}_{\mathcal{M}}\mathcal{S}$ - $\mathbb{A}^{T}_{\mathbf{E}}X$. Akademisk avhandling som med tillstånd av Kungliga Tekniska Högskolan i Stockholm framlägges till offentlig granskning för avläggande av teknologie doktorexamen torsdagen den 16:e Juni 2005 kl 10.00 i salen D2, Kungliga Tekniska Högskolan, Lindstedtsvägen 5, Stockholm. ©Olivier Macchion 2005 Intellecta Docusys, Stockholm 2005



CFD in design of gas quenching furnaces.

Olivier Macchion

Faxénlaboratoriet Department of Mechanics, Royal Institute of Technology SE-100 44 Stockholm, Sweden.

Abstract

This thesis focus on the numerical study of gas quenching within industrial furnaces. Gas quenching is the rapid cooling of metal pieces, aiming at performing a transformation of the metal structure to improve its mechanical properties. In the present study, several aspects of the factors influencing the performance of a gas quenching furnace have been studied. A first study focused on the flow and heat transfer fields both in an empty furnace and in a furnace loaded with different charges. The objective was to study the influence of the charge configuration on the flow and heat transfer uniformity. This study led to the identification of several possible improvements, and these improvements are currently being implemented by the industrial partners of this project. As earlier studies had shown the importance of flow uniformity on the quality of the heat treatment, a second work focused solely on the flow uniformity upstream of the quenching zone. This led to the writing of design recommendations for this particular type of furnace. Investigations of the dependence of the performance of the coolant on gas composition were performed. Improved knowledge of the effect of gas mixture composition on heat transfer was added to the body of knowledge already available. Further studies of the factors suspected to be of influence have been performed, leading to the identification of several avenues for future research.

Descriptors: Gas quenching, modeling, CFD, gas mixtures, uniformity.

Preface

This thesis treats hydrodynamics and heat transfer within gas quenching furnaces, both from an economical point of view through the estimation of the pressure drop occurring during such processes, and from a quality point of view through the estimation of the heat treatment uniformity. The research was conducted within the framework of Faxénlaboratoriet, a centre of excellence located at the Royal Institute of Technology in Stockholm, Sweden. The thesis is divided in two main sections. In the first of these, an introduction is given to the science of metal hardening, called quenching. A summary of the research conducted by the thesis author and his co-workers is also given, with the objective to clarify its context. The second part consists of the appended scientific papers. When necessary, these have been reset in the format of this thesis.

Stockholm, June 2005. Olivier Macchion

Appended papers:

furnace'

Paper 1. Macchion, O. and Zahrai, S. and Bouwman, J. 2004 'On hydrodynamics within gas quenching furnace' Submitted to the Journal of Materials Processing Technology.

Paper 2. Macchion, O. and Zahrai, S. and Bouwman, J. 2004 'On heat transfer within gas quenching furnace' Submitted to the Journal of Materials Processing Technology.

Short version published in the IASME Transactions vol. 1(2), January 2005

Paper 3. Macchion, O. and Zahrai, S. 2004 'CFD for design of gas quenching

Proceedings of the 17th Nordic Seminar on Computational Mechanics, pp.62-65

Paper 4. Macchion, O. and Lior, N. 2004 'Computational study of velocity distribution for designing some gas quench chamber and furnace ducts' Published in the Journal of Materials Processing Technology, Vol. 155-156, November 2004, p.1727-1733

Paper 5. Macchion, O. and Zahrai, S. 2004 'On the influence of gas mixture composition on gas quenching uniformity and mean'

Accepted for presentation at the ASME Heat Transfer Conference 2005, in San Francisco.

Submitted for publication in the ASME Transactions, Journal of Heat Transfer.

Paper 6. Macchion, O. and Zahrai, S. 2004 'Heat transfer correlation within gas quenching chamber'

Submitted to the International Journal of Heat and Fluid Flow.

Paper 7. Macchion, O. and Zahrai, S. 2005 'Large eddy simulation of flow and heat transfer over a cylinder in axial flow' Draft.

Papers not present in this thesis

Ko, J. and Macchion, O. and Zahrai, S. 2004 'Numerical Modeling of High Swirl Flows in a Through-Flow Cylindrical Hydrocyclone' Submitted to the American Institute of Chemical Engineers Journal.

Ko, J. and Macchion, O. and Zahrai, S. 2004 'Numerical Modeling of Swirling Turbulent Pipe Flows Created by Tangential Inlets' Submitted to the International Journal for Numerical Methods in Fluids.

Division of work between authors

The work presented in this thesis has been done in collaboration with other researchers. The respondent performed the major part of the work. Prof. Said Zahrai, Department of Mechanics KTH, Prof. Noam Lior, Pennsylvania State University, Dr. Jan Bouwman, Dr. Anders Åström have acted as supervisors. They have all contributed with comments and discussion of the work and the manuscripts.

Parts of the activities have been presented in talks given at,

The AMPT 2003, Dublin, Ireland, in July 2003,

Svenska Mekanikdagar, Gothenburg, Sweden, in August 2003

The 17th Nordic Seminar on Computational Mechanics, Stockholm, Sweden, in October 2004,

The 2005 IASME Heat Transfer Conference, Udine, Italy, 20-22 January 2005,

Contents

Preface	vii
Chapter 1. Introduction	1
1.1. Heat treatment of steels	1
1.1.1. Heating temperatures and phase transformation	1
1.1.2. Cooling rate and phase transformations	3
1.2. Quenching	5
Chapter 2. Quenching chamber and performance parameters	8
2.1. Gas quenching furnaces	8
2.2. Architecture of the VUTK furnace	10
2.3. Heat transfer modes in a gas quenching furnace	12
2.4. Convective heat transfer and fluid properties	15
2.5. Heat transfer uniformity	15
Chapter 3. Mathematical modeling of flow and heat transfer	17
3.1. Gas properties	18
3.1.1. Pure gases	18
3.1.2. Mixtures of pure gases	19
3.2. Turbulence modeling	20
3.2.1. Shear-Stress Transport model	20
3.2.2. Differential Reynolds Stress model	22
3.3. Solution methodology	23
Chapter 4. Summary of results	24
4.1. Heat transfer around a cylinder in axial homogeneous flow	24
4.2. Influence of quenching basket on heat transfer	26
4.3. The influence of gas mixture composition	29
4.4. Gas quenching furnace	30
4.4.1. Validation of the computational model	31
4.4.2. Multi-body charges	32

x CONTENTS

4.5	5. Chamber geometrical characteristics and chamber performance	36
4.6	6. Flow uniformity and duct geometry.	39
4.7	7. Flow uniformity upstream of the charge.	41
Chaj	pter 5. Concluding remarks	42
Ackı	nowledgments	45
Bibli	iography	46
On l	nydrodynamic effects within gas quenching furnace	51
1.	Introduction	51
2.	Problem statement	54
3.	Mathematical model	55
4.	Numerical method and boundary conditions	58
5.	Results and analysis	59
6.	Summary and conclusions	64
Re	eferences	66
On l	neat transfer within gas quenching furnace	69
1.	Introduction	69
2.	Problem statement	70
3.	Mathematical formulation and mumerical method	72
4.	Results	73
5.		81
Re	eferences	82
\mathbf{CFD}) for design of gas quenching furnace	87
1.	Introduction	87
2.	Computational method	88
3.	Hydrodynamics within the quenching chamber	88
4.	Heat transfer within the quenching chamber	89
5.	Quenching basket design	90
6.	Concluding remarks	90
Re	eferences	91
Com	aputational study of velocity distribution for designing some gas quench chamber and furnace ducts	95
1.	Introduction	95 95
1. 2.		95 97
۷.	2.1. Transition Duct Model Configurations	97
	2.2 Solver and Boundary Conditions	98

	CONTENTS	s xi
	2.3. Performance Criteria	99
2	Circular-to-rectangular transition ducts	100
ა.	<u> </u>	100
	3.1. Duct length effects	100
	3.2. Duct Exit Aspect Ratio (A/R) Effects	_
	3.3. Expanding-Contracting Duct	102
	3.4. Pressure effects	103
4	3.5. Reynolds number effects	103
4.	Ducts bends	105
	4.1. Geometry and Computational Model	105
_	4.2. Results	105
5.	Conclusions and recommendations	106
6.	Acknowledgements	106
$R\epsilon$	eferences	106
Inve	stigation of the influence of gas composition on heat uniform	nity
	and mean	111
1.	Introduction	111
2.	Problem statement	112
3.	Mathematical model	114
4.	Numerical method	115
5.	Results	117
6.	Conclusion	123
Ac	cknoledgements	124
$R\epsilon$	eferences	124
Нова	t transfer correlation within gas quenching furnace	129
1.	Introduction	$\frac{129}{129}$
2.	Problem statement	131
3.	Mathematical model	133
3. 4.	Boundary conditions and numerical method	133
5.	Results	134
6.	Discussion, recommendation, and future work	134 142
_	cknowledgments	144
	eferences	144
116	eierences	144
Larg	ge eddy simulation of flow and heat transfer over a cylinder	\mathbf{er}
	in axial flow	149
1.	Introduction	149
2.	Problem statement	150
3.	Mathematical model	151

xii CONTENTS

4.	Numerical method	152
5.	Results	153
6.	Conclusion	157
Ac	cknowledgements	159
References		159

CHAPTER 1

Introduction

This thesis is concerned with flow and heat transfer modeling for the hardening of metal pieces by gases. To set the stage for the presentation of the work that has been undertaken, I therefore think it is appropriate to dedicate the first chapter of this thesis to an introduction to the science of phase transformation within metals. As will become evident, the cooling process is given a more lengthy presentation, since it has been the main focus area of the conducted research.

1.1. Heat treatment of steels

Most carbon, low-alloy, high-alloy steel and ceramic parts produced today are heat treated, both to enhance particular properties, such as hardness, toughness, and corrosion resistance, and to improve uniformity properties. The treatment depends on both the type of alloy and the intended service consitions. In general heat treatment is an operation involving heating to an elevated temperature followed by controlled cooling to obtain particular microstructures and combinations of properties. The utility of steel lies largely in the relative ease with which properties can be altered by controlling the way parts are heated and then cooled. The changes in properties occur principally because different microstructural constituents are achieved with different cooling rates. A good description of the operations performed during heat treating of steel is available in Totten et al. (1993).

1.1.1. Heating temperatures and phase transformation

Most carbon and low-alloy steels contain less than 0.83 % C. As a consequence the microstructure is a two-phase mixture consisting of α iron, also called ferrite, and perlite. Ferrite is a body-centered cubic (bcc) phase, and perlite is a mixture of ferrite and cementite, Fe_3C , existing as alternating lamellae. If such a steel is heated to a moderate temperature of about 425 to 650 °C (800 to 1200°F), internal stresses may be relieved without substantially altering the microstructure or physical properties.

The iron-carbon phase diagram is shown in figure 1.1. The iron-carbon diagram is a map that depicts the phases present as a function of carbon concentration and temperature. At carbon concentrations below about 0.83 % and temperatures below the eutectoid value of 720 o C (1330 o F), the stable phases are ferrite and perlite. At carbon concentrations above about 0.83

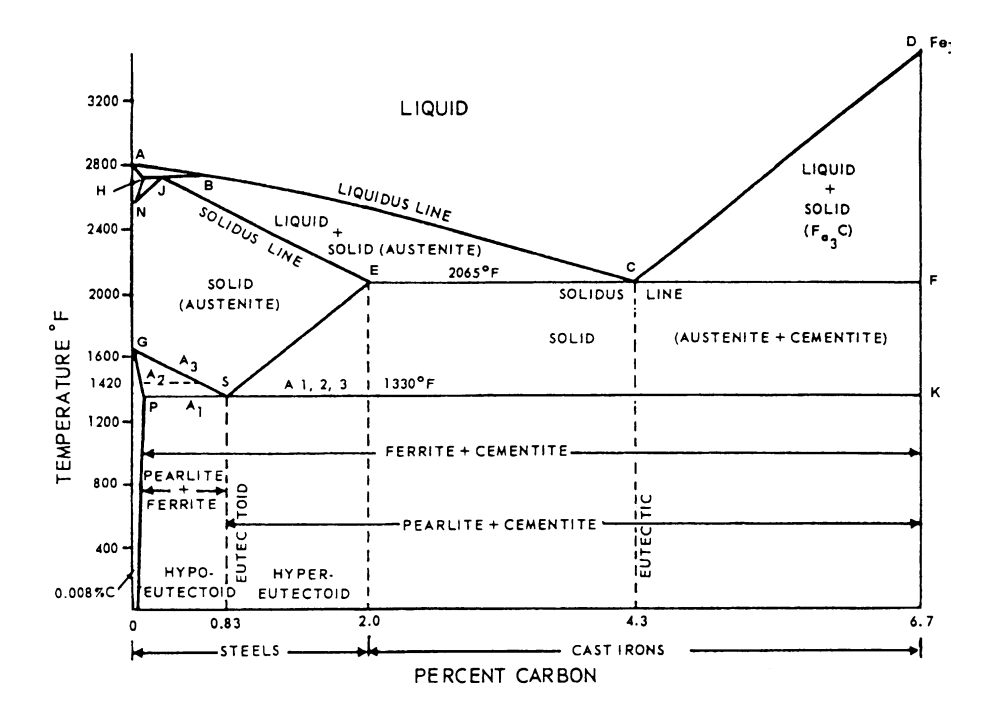


FIGURE 1.1. Iron-carbon phase diagram

% and below 2 %, the stable phases below 720°C (1330°F) are perlite and cementite. At carbon concentrations above 2 %, the metal is called cast-iron, and its structure and phases change.

If a steel containing less than the eutectoid carbon concentration is heated to a temperature just above the eutectoid temperature, perlite decomposes to produce face-centered cubic austenite, called γ iron, resulting in a mixture of ferrite and austenite phases. If heating is continued to higher temperatures, the ferrite progressively decomposes to form more austenite. At a sufficiently high temperature, the ferrite and any carbides present are completely decomposed to produce a homogeneous austenitic microstructure. This heating process is called solution heating or austenitizing. The upper critical temperature for a steel containing less than 0.83 % C is represented by the line G-S on figure 1.1.

Heating a carbon steel containing more than about 0.83 % C to a temperature above the eutectoid value again results in decomposition of the perlite to form austenite and produces a structure containing both austenite and cementite. At higher temperatures, the cementite is progressively decomposed until, at a sufficiently high temperature, the structure consists of homogeneous austenite. The upper critical temperature for a steel containing more than 0.83 % C is represented by the line S-E in figure 1.1. The lower critical temperature for both hypoeutectoid and hypereutectoid steels is represented by the line P-S-K.

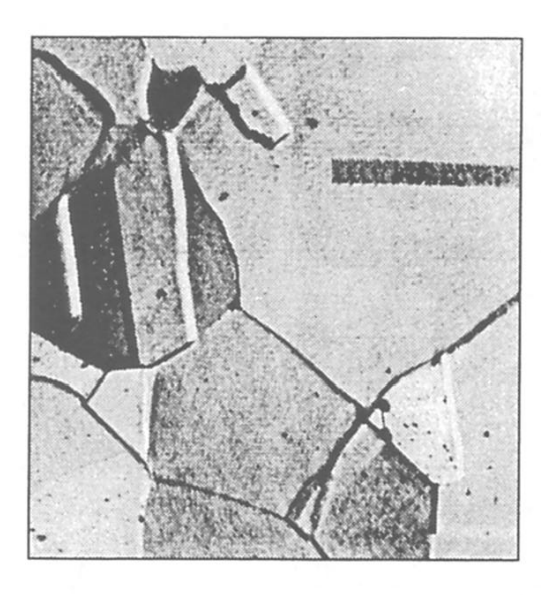


FIGURE 1.2. Microscopic structure called austenite magnified 500 times.

Induction heating and radiation heating are two of the most used heating methods. Induction heating is the process of heating a metal object by placing a wound coil carrying high alternating current at close proximity to the object to be heated. This technology is being adopted into the domestic kitchen heating in the form of the induction cooker. This process can also be used for eliminating unwanted oxygen gas in vacuum tubes and for high volume industrial welding.

Radiation heating consists in using the propagation of heat through infrared waves to heat up the metal pieces from within the quenching chamber. Other methods include flame heating, laser beam heating, and electron beam heating.

1.1.2. Cooling rate and phase transformations

If a solution-treated steel, also called austenitized steel, containing less than about 0.83~% C is slowly cooled from the austenite temperature region, the first phase to precipate from the austenite is ferrite. This transformation results in a change in the atomic arrangement from the fcc austenite to bcc ferrite. Because ferrite can dissolve only a small amount of carbon, the concentration of carbon in austenite increases during cooling, until at the eutectoid temperature of about of about 720~% (1330%F), the remaining austenite transforms to perlite.

4 1. INTRODUCTION



FIGURE 1.3. Microscopic structure called martensite magnified 2500 times.

Slow cooling a hypereutectoid steel containing more than 0.83 % C is similar to cooling a lower-carbon steel, except that the first constituent to precipitate from austenite is cementite. Cementite usually forms at austenite grain boundaries and forms a network structure that can be observed in the steel at room temperature after the transformation is complete. At exactly the eutectoid composition, austenite decomposes into pearlite without the formation of either primary ferrite or primary cementite.

Because both ferrite and perlite formation requires some diffusion of carbon, higher cooling rates reduce the thickness of the ferrite and cementite phases in perlite. In general, higher cooling rates produce thinner lamellae, which in turn produce a progressive increase in hardness and strength.

At even higher cooling rates, it is possible to avoid the transformation of austenite to ferrite and perlite in many carbon and low-alloy steels. The transformation of austenite at temperatures below 540 °C (1000°F), but above about 200°C (400°F), produces a structure composed of ferrite and cementite, but the phases are not arranged in a lamellar form. Instead the ferrite and cementitehave a feathery or acicular appearance, and neither constituent can be clearly resolved with an optical microscope. These structures are known as bainite.

Transformation of austenite at even lower temperatures, below about 200°C (400°F), produces a body-centered tetragonal (bct) structure called martensite, which is found in fully hardened steels. Microstruturally, martensite has

a needlelike appearance, as illustrated in figure 1.3. The formation of martensite necessitates severe quench, and suppresses the formation of ferrite, perlite, and bainite. Because martensite occupies a greater volume than austenite, steel expands when martensite forms and results in dimensional changes that may cause distortion. In severe situations, distortion may cause parts to crack during quenching.

1.2. Quenching

The most common method of hardening steel involves continuously cooling from the solution treating (austenitizing) temperature in a liquid that rapidly extracts heat. The rate of cooling in the part depends on the heat removal characteristics of the cooling medium, the thermal characteristics of the alloy, and the section thickness of the part. At a sufficiently high rate of cooling, transformation does not occur until the M_S temperature is reached and martensite formation begins ¹. Such cooling conditions will produce a fully hardened steel, and is called the critical cooling rate. A cooling rate slower than the critical value will allow formation of some bainite or perlite and thus will not produce full hardening.

Air cooling, gas quenching, oil quenching, water quenching, and spray quenching are different means of obtaining cooling rates of different magnitude. It is generally admitted, as expressed by de Oliveira et al. (2002), that oil quenching and water quenching lead to the development of high residual stresses in the component. These in turn can cause distortion during the final machining operations or after the quenched part is put into service. As an alternative, if the part are sufficiently thin, forced convective gas cooling can be used to provide an appropriate cooling rate. For thicker parts, pressurized gas quenching is a solution of choice.

Figure 1.4 show some metal parts that have first been carburized, and then gas quenched. Use of gas as quenching medium has been suggested, investigated and used during the past years. Gas quenching has a number of advantages in comparison with conventional methods. The elimination of quenching oils makes gas quenching an environmentally friendly process with no emissions to air and water and, in addition, without any need for post-washing or systems for oil disposal. Eliminating oil and salt baths also improves the working conditions with regard to safety, since it eliminates fire hazards and toxic gases. Compared to oil quenching, the controlled cooling rate for a gas quenching system improves the product quality with better controlled and reduced distortions, see e.g. Troell & Segerberg (1995). This all leads to better process economics, since the cost of washing is eliminated, the amount of grinding is reduced and the associated costs for handling waste are decreased.

Gas quenching furnaces can be grouped into two main types: single chamber vacuum furnaces and double chamber vacuum furnaces. In the former one the charge is heated and cooled in the same chamber, while in the latter one

¹The M_S temperature is defined as the temperature where martensite formation begins.



(a) Automotive ring gears vacuum carburized at 1230 K in 114 min cycle with 15 bar nitrogen quench



(b) Helical shafts carburized at 1230 K in 114 min cycle with 8 bar nitrogen quench



(c) Helical gears carburized at 1230 K in 114 min cycle with 12 bar nitrogen quench



(d) Vacuum carburized ring gears

FIGURE 1.4. Examples of carburized and gas quenched metal pieces.

the charge is heated in the first chamber, and cooled in the second, thus providing potentially higher cooling rates. The gas quenching furnace uses usually a closed loop system where a fan pumps the gas through the quenching chamber where the hot parts to quench are placed. The gas flows after the quenching chamber through a water-cooled heat exchanger, and back to the fan inlet. An example of single chamber vacuum furnace is the VUTK furnace discribed in Bless & Edenhofer (1997), a schematic skiss of which is presented in figure 2.6.

Usually, a large number of metal parts are simultaneously cooled in a gas quenching furnace. To achieve a high quality of the quenched products, the heat removal must be uniform both across the whole charge and around each part. These two issues must be considered in both design of the furnace and the arrangement of the parts relative to each other in the charge basket.

Thuvander et al Thuvander et al. (1998) studied the gas quenching process and showed how flow homogeneity influences the uniformity of the mechanical properties, in particular the hardness, of gas-quenched metal parts. Two main factors can contribute to the lack of flow uniformity in a gas quenching furnace. Firstly, the design of the furnace must insure a uniform distribution of flow around the charge. The design of the furnace usually reflects consideration of a large number of factors such as cost, weight and size. Strong optimization with respect to other factors can sometimes result in complex flow paths giving rise to strong variations in the gas velocity. Secondly, as most bodies to quench are bluff bodies, occurance of flow separations results in local varition of heat transfer properties. See e.g. Igarashi (1981), Roshko (1955), Roshko (1993), and Koenig & Roshko (1985).

The aim of this thesis is to present a review of the phenomena taking place within a gas quenching chamber, from a fluid dynamics and heat transfer perspective. For a start one considers the hydrodynamics and heat transfer within a gas quenching chamber, with a focus on the emergence of non uniformities both within the flow and heat transfer fields. Then the focus is put on how gas mixtures may affect the global performance of a gas quenching furnace, both in terms of mean and uniform heat transfer.

In the present chapter, chapter 1, the process of gas quenching has been introduced. In chapter 2 the fundamentals of the gas quenching process and of the design of a gas quenching chamber are presented. Chapter 3 presents the mathematical models that underlines the study of such flows numerically. In chapter 4, a summary of papers 1 to 8 is performed, with a focus on the flow and heat transfer around bluff bodies, the flow and heat transfer in a gas quenching chamber, and the influence of the design of the entrance to the furnace on the flow homogeneity at its exit plane. Finally, chapter 5 summarizes the studies that were performed in the course of this thesis, and gives a perspective on future research on the topic of gas quenching. Aspects of the applicability of the work performed here to the more general industry of gas cooling are considered.

CHAPTER 2

Quenching chamber and performance parameters

2.1. Gas quenching furnaces

The metal pieces to quench are characterized by a large diversity of shapes and dimensions. As it can be seen on figures 2.1(a), 2.1(b), 2.1(c), and 2.1(d), the dimensions and number of pieces to quench can vary a lot, going from a few centimeters to the order of the meter. Quenching furnace manufacturers solve this problem by making available different furnace architectures specifically manufactured for a kind of metal pieces, and for different cooling rates. To help the reader in following the discussion presented in this work, a few terms proper to quenching manufacturer jargon are defined. The term single-chamber furnace refers to furnaces where the heating to solution-treating temperature and quenching occur in the same chamber. The term two-chambers furnaces refers to furnaces where heating and quenching take place in two adjoining chambers, as in the VAK furnace presented in figure 2.2.

On figure 2.3, two examples of furnace construction are presented. The furnaces presented in figure 2.3 have the specific features of all single-chamber quenching furnaces, and which are (1) a fan, (2) a heat exchanger, (3) an inner chamber. The heating and quenching processes take place in the inner chamber, where heating resistances will provide the electromagnetic energy necessary to the heating process. The differences between the two architectures presented in figure 2.3 lie in the cooling apparatus. In the VUTK furnace presented in figure 2.3(a), the cooling is performed by a column of high velocity flow driven from the top to the bottom of the quenching chamber by the fan. In the VRK furnace presented in figure 2.3(b), the cooling is performed by a series of nozzles placed on the periphery of the quenching chamber, also called heating zone.

The different types of furnaces are manufactured for specific needs and piece shapes. For instance the VUTK furnace, presented in schematic form on figure 2.3(a), is specifically well suited for long pieces like the cylinders presented in figure 2.4. While the furnace of the type presented in figure 2.5 are specially well suited for quenching of large metal pieces, as the flow comes from different directions through directing nozzles.

In this work, the focus was set on the VUTK furnace. The VUTK furnace is a single chamber furnace, which is a concept that IPSEN International GmbH has found to be of great interest as it involves reduced size and weight compared to the other types of furnaces presented earlier. At the same time it presents a



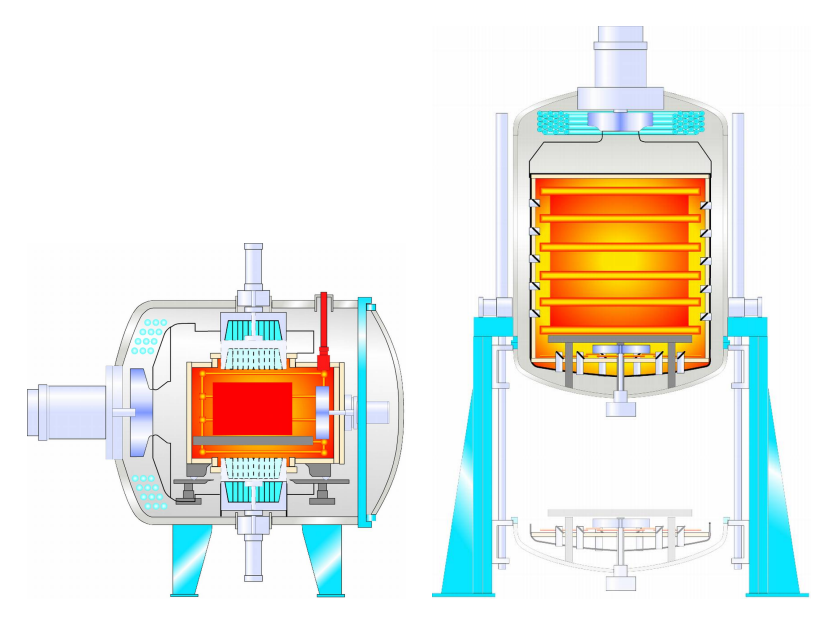
FIGURE 2.1. Charges of different dimensions and shapes.

(d) Large object.

(c) Chains



FIGURE 2.2. Two-chamber VAK furnace.



- (a) VUTK furnace.
- (b) VRK furnace, based on the use of multi-directional nozzles.

FIGURE 2.3. Charges of different dimensions and shapes.



FIGURE 2.4. Cylinders.

challenge due to the numerous constraints that its design must satisfy. In the following section the purpose and constraints set on the design of the VUTK furnace are presented.

2.2. Architecture of the VUTK furnace

In this section we focus on the architecture of the VUTK furnace as presented by Bless & Edenhofer (1997). This furnace is found to be representative of a type of furnaces that have been recognized as particularly interesting from a



FIGURE 2.5. Relative dimensions of the charge and the furnace.

commercial point of view, namely single chamber furnaces, even if double chamber furnaces have been shown to lead to better quenching behavior. Figure 2.6 presents the flow path from the fan exit to the fan inlet, i.e. the physical domain considered in this thesis. The gas flowing out from the chamber is cooled off by an external heat exchanger and is pumped back into the external chamber by a fan. This external chamber separates the pressurized fluid from the outer atmosphere. The quenching chamber, i.e. the chamber where the quenching process takes place, has a parallelepipedic shape with two rectangular openings opposing each other. The one through which the gas enters the chamber is usually called the entrance box and the other is called the exit trap.

The advantages of quenching in furnaces like the VUTK furnace are twofold: (1) a single batch can contain many elements, (2) the architecture is favorable to the execution of pre-treatments like carburizing, followed by gas quenching.

The heat treatment process as performed today consists in the following stages:

- The load is placed within the chamber, and both entrance and exit traps are closed.
- 2. The air is pumped out and vacuum is provided.
- 3. Heating by radiation is performed until the solution treating temperature is reached.
- 4. The entrance box containing the tube bundle aiming at straightening the flow is lowered over the entrance trap, and at the same time the fan is put into rotation.
- 5. The coolant fills the furnace. This operation takes only a few seconds.
- 6. The coolant flows from the entrance box through the charge and exits through the exit trap for 20 seconds.

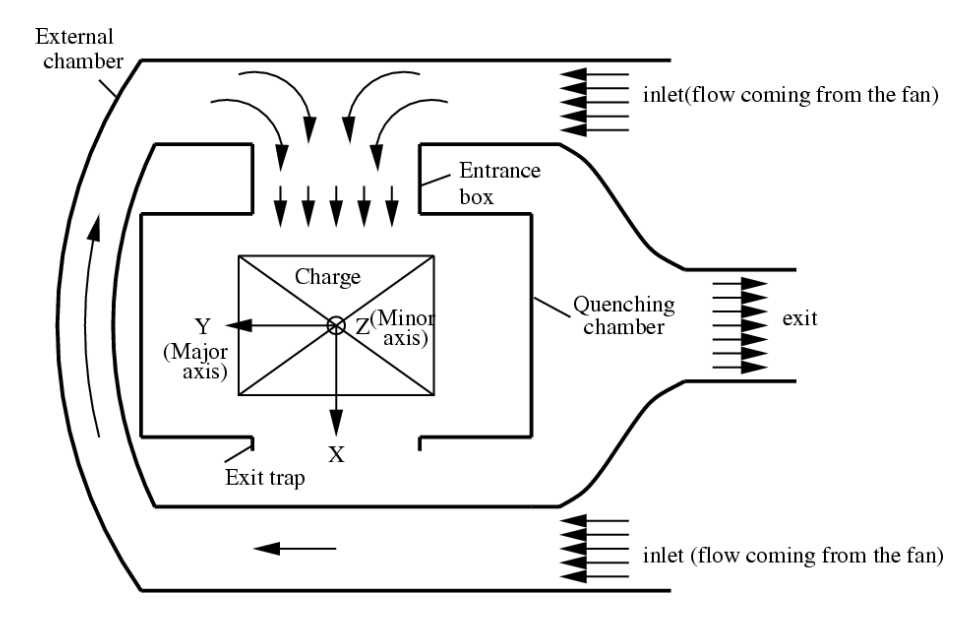


FIGURE 2.6. Quenching chamber and its surroundings - the gas coming from the fan enters the furnace through a circular vent, moves through the whole external chamber, goes through the entrance box, goes through the charge, and finally exists through the exit trap to get back to the fan.

- 7. After 20 seconds, the tube bundle is retracted, the entrance is connected to the inlet to the fan and thus becomes the exit trap, while the former exit trap becomes the entrance trap for this cycle as the opposite tube bundle is lowered.
- 8. This alternating cycle is repeated for five to ten minutes, depending on the type of steel and load.

In the following the flow and heat transfer in the VUTK furnace architecture that was presented here are studied.

2.3. Heat transfer modes in a gas quenching furnace

Practitioners of the thermal arts and sciences generally deal with four basic thermal transport modes: conduction, convection, and radiation. The process by which heat diffuses through a solid or a stationary fluid is termed heat conduction. Situations in which heat transfer from a wetted surface is assisted by the motion of the fluid give rise to heat convection. The exchange of heat between surfaces, or between a surface and a surrounding fluid, by long-wavelength electromagnetic radiation is termed thermal heat radiation.

In a gas quenching furnace, the application of interest in this thesis, the domain of temperatures is such that heat transfer by radiation is of importance only in an early stage of the quenching process. Only heat transfer by conduction within the metal and by convection between the metal to be quenched and the quenching fluid is of interest in the present study.

Thermal conduction within a solid body to quench is governed by Fourier's law of conduction.

$$q = -k\nabla T, (2.1)$$

where q is the heat flux, expressed in W·m⁻², k is the thermal conductivity of the material, and T is the temperature, expressed in Kelvins, K.

Convective thermal transport from a surface to a fluid in motion can be related to the heat transfer coefficient h, the surface-to-fluid temperature difference, and the wetted surface area S in the form

$$q = hS(T_s - T_f). (2.2)$$

The differences between convection to a rapidly moving fluid, a slowly flowing fluid, or a stagnant fluid, as well as variations in the convective heat transfer rate among various fluids, are reflected in the values of h. For a particular geometry and flow regime, h may be found from available empirical correlations, theoretical relations, or, as it has been done in this study, by solution of the equations of motion and energy presented in chapter 3.

Common dimensionless quantities that are used in the correlation of heat transfer data are the Nusselt number Nu, which relates the convective heat transfer coefficient to the conduction in the fluid:

$$Nu \equiv \frac{h}{k/L} = \frac{hL}{k} \tag{2.3}$$

The Prandtl number Pr, which is a fluid property parameter:

$$Pr \equiv \frac{C_p \mu}{k} = \frac{\nu}{\alpha} \tag{2.4}$$

and the Reynolds number Re, which relates the momentum in the flow to the viscous dissipation:

$$Re \equiv \frac{\rho U_b L}{\mu} \tag{2.5}$$

All thermal properties in the foregoing dimensionless groups apply to the fluid at its bulk temperature. The quantity L is a characteristic dimension of the system under consideration, and U_b is the bulk velocity of the fluid in motion.

Other numbers, like the Grashof number Gr, which accounts for the buoyancy effect:

$$Gr \equiv \frac{\rho^2 \beta g L^3 \Delta T}{\mu^2} \tag{2.6}$$

have been introduced to characterize systems where no fan is forcing the flow. In gas quenching furnaces, flow velocities are within the range 15-30 m·s⁻¹, which lead to Reynolds numbers of the order $Re=10^6$ for air and at high pressure, P=10 bar for instance. This means that the buoyancy effects can be safely neglected. This affirmation can be shortly demonstrated by taking

the ratio of the buoyancy and inertia forces, which are of equal magnitude in the case of a vertical wall if

$$\frac{-\left(\rho_0 - \rho_\infty\right)g}{\rho_\infty U_\infty^2/L} \sim 1. \tag{2.7}$$

In terms of Grashof and Reynolds number, this translates into

$$\frac{Gr}{Re^2} \sim 1\tag{2.8}$$

Therefore, if $Gr/Re^2 \ll 1$, then the buoyancy forces will be much smaller than the inertia forces. The flow will be determined by the inertia and friction forces. In the case of free convection, $Gr/Re^2 \gg 1$, and the buoyancy forces are much larger than the inertia forces. The flow is determined by the buoyancy and friction forces. In gas quenching furnaces, the typical Reynolds number is $Re = 10^6$, while the Grashof number is of order unity.

Laminar flows are structured, ordered flows, where the direction of motion at any point remains constant as if the fluid were moving in a series of layers sliding over one another without mixing. Beyond a critical Reynolds number, usually of order 10^3 , the flow begins to lose its organized structure and becomes turbulent. The structure of a turbulent flow, its behavior, and its effects on heat and mass transfer change drastically when compared to a laminar flow in the same geometrical set-up. As written earlier, the typical Reynolds number in a gas quenching furnace is $Re = 10^6$.

According to Tennekes & Lumley (1972) , the main features of turbulence are

- 1. Randomness of the turbulent fluctuations.
- 2. Diffusivity that causes mixing and improves the momentum, mass and heat exchange.
- 3. The large Reynolds number range where such turbulence occurs.
- 4. The three dimensional characteristic of the fluctuations with transfer of turbulence between the directions.
- 5. The dissipation which occurs at the end of the turbulent cascade and which smoothes the fluctuations under the turbulent ultimate length scale.
- 6. The continuum characteristics of this ultimate length scale is higher than a molecular mean free path and allows a treatment through the general continuum mechanics equations.
- 7. Turbulence is induced by the flow configurations and not by a physical property of the fluid. This feature should be kept in mind as it gives rise to the underlying hypothesis of the different turbulence models.

One of the main features pointed out by Tennekes & Lumley (1972) is the fact that turbulence should improve the heat exchange between the fluid used as quenchant and the metal pieces to quench. Numerous experimental evidence of such phenomenon has been given. Some good references are the works performed by Hunt (1973), Arts et al. (1990), Hancock & Bradshaw (1983),

Van Fossen & Ching (1994), Van Fossen & Simoneau (1994), Van Fossen et al. (1995), and Butler et al. (2001). The studies reviewed evidenced the influence of turbulence on heat transfer and the influence that surfaces and strain fields have on turbulence.

2.4. Convective heat transfer and fluid properties

TABLE 2.1. Mean heat transfer coefficient at 10 bar, $15 \text{ m} \cdot \text{s}^{-1}$, cross-flow of cylinders with diameter 28 mm.

Properties	Argon	Nitrogen	Helium	Hydrogen
ρ	1.669	1.170	0.167	0.084
C_p	523	1040	5190	14300
k	0.0173	0.0255	0.1536	0.1750
μ	$23 \cdot 10^{-6}$	18.10^{-6}	20.10^{-6}	9.10^{-6}
Re				
h	360	500	775	950

Table 2.1 presents the heat transfer coefficients calculated using the relation presented by Zukauskas (1987), for tube bundles in cross-flow. ρ is the density, $kg\cdot m^{-3}$, C_p the specific heat capacity, $J\cdot kg^{-1}\cdot K^{-1}$, k the thermal conductivity, $W\cdot m^{-1}\cdot K^{-1}$, μ the dynamic viscosity, $N\cdot s\cdot m^{-2}$, and h, $W\cdot m^{-2}\cdot K^{-1}$, the heat transfer coefficient, as said earlier in this chapter. From this table, it is obvious that the choice of the gas has a strong influence on the performance of the quenching process. Studies of this dependence are presented in chapter 4 and in the work by Macchion $et\ al.\ (2004b)\ (Paper\ 5)$.

2.5. Heat transfer uniformity

Thuvander et al. (1998) studied the gas quenching process and showed how flow homogeneity influences the uniformity of the mechanical properties, in particular the hardness, of gas-quenched metal parts. Most of this work has focused on determining how the quenching chamber geometry and fluid properties affect the heat transfer uniformity over the bodies to quench, and the flow uniformity around them.

Different criteria have been developed in the literature and considered in this work to evaluate the uniformity of a flow. Lefantzi & Knight (2002) studied the flows in subsonic S-shaped diffusers. The measure of merit that they used in their study is the so-called total pressure distortion index described over the two-dimensional circular domain at the exit of the diffuser. This total pressure distortion index can be thought of as the maximum total pressure difference over the cross-section of interest. Anon (1978a,b) developed a criterion based on three quantities giving the intensity, extent, and multiple-per-rev values of the distortion. The intensity describes the magnitude of the distortion. The

extent describes the area covered by a low-pressure region, and the multipleper-rev value describes the number of low-pressure regions there are in one 360-deg revolution.

These criteria were found to give a very good overview of the flow uniformity, but were difficult to implement over complex geometries. Measures of uniformity like the standard deviation, presented in equation (2.9), constitute a sufficiently good judge of the uniformity of a flow field.

$$N = \frac{1}{u_{avg}} \sqrt{\frac{1}{S} \int_{S} (u - u_{avg})^{2} dS},$$
 (2.9)

The uniformity of a heat transfer field is difficult to estimate without performing a calculation of the residual stresses inside the metal that is to be quenched. However, Thuvander et al. (1998) established that a uniform flow will result in lower residual stresses, and as such it was decided to focus the work on finding out which parameters would influence in a beneficial way flow uniformity.

CHAPTER 3

Mathematical modeling of flow and heat transfer

In this thesis the turbulent flow of a viscous, incompressible fluid is considered. The hydrodynamics of the flow field is described by the Navier-Stokes equations

$$\rho \left(\frac{\partial \tilde{u}_i}{\partial t} + \tilde{u}_j \frac{\partial \tilde{u}_i}{\partial x_i} \right) = -\frac{\partial \tilde{p}}{\partial x_i} + \mu \nabla^2 \tilde{u}_i, \tag{3.1}$$

and the continuity equation

$$\frac{\partial \tilde{u}_i}{\partial x_i} = 0, \tag{3.2}$$

where ρ is the density of the fluid, μ is the kinematic viscosity of the fluid, and x_i is the spatial coordinate. Note that the Einstein notation is applied in all equations.

The thermal field is described by the energy equation

$$\rho C_p \left(\frac{\partial T}{\partial t} + \tilde{u_i} \frac{\partial T}{\partial x_i} \right) = \frac{\partial}{\partial x_i} \left(k \frac{\partial T}{\partial x_i} \right). \tag{3.3}$$

where T is the temperature of the fluid, and k is the thermal conductivity of the fluid.

Velocity, pressure, and temperature are decomposed into mean and fluctuating parts as

$$\tilde{\phi} = \Phi + \phi, \tag{3.4}$$

where Φ denotes the mean value of the flow or temperature variable. For general turbulent flows that are neither statistically steady not homogeneous, the mean value of any variable ϕ is taken to be the ensemble average

$$\overline{\phi} = \overline{\phi}^{(E)}(\mathbf{x}) = \lim_{N \to \infty} \frac{1}{N} \sum_{k=1}^{N} \phi(\mathbf{x}, t)^{(k)}, \tag{3.5}$$

where the average is taken over N repeated experiments. The mean value of a statistically steady turbulent variable ϕ can simply be taken to be the time average

$$\overline{\phi} = \overline{\phi}^{(T)}(\mathbf{x}) = \lim_{T \to \infty} \frac{1}{2T} \int_{-T}^{T} \phi(\mathbf{x}, t) dt, \tag{3.6}$$

whereas for spatially homogeneous turbulence, a volume average can be used,

$$\overline{\phi} = \overline{\phi}^{(V)}(\mathbf{x}) = \lim_{V \to \infty} \frac{1}{V} \int_{V} \phi(\mathbf{x}, t) d^{3}x. \tag{3.7}$$

The ergodic hypothesis is assumed to apply, namely, that in a statistically steady turbulent flow, it is assumed that

$$\overline{\phi}^{(T)} = \overline{\phi}^{(E)},\tag{3.8}$$

and in a homogeneous turbulent flow is assumed that

$$\overline{\phi}^{(V)} = \overline{\phi}^{(E)}. \tag{3.9}$$

The Reynolds-averaged Navier-Stokes equations, which physically corresponds to the conservation of mean momentum, takes the form

$$\rho U_j \frac{\partial U_i}{\partial x_j} = -\frac{\partial P}{\partial x_i} + \mu \nabla^2 U_i - \rho \frac{\partial \overline{u_i u_j}}{\partial x_j}, \tag{3.10}$$

where $\overline{u_i u_i}$ is the Reynolds-stress tensor. Equation 3.10 is obtained by substituting the decomposition 3.4 into the Navier-Stokes equations 3.1 and then taking an ensemble average. The mean continuity equation is given by

$$\frac{\partial U_i}{\partial x_i} = 0, (3.11)$$

and is obtained by taking the ensemble average of equation 3.2.

The steady energy equation is given by

$$C_{p} \frac{\partial}{\partial x_{i}} \rho U_{i} T = \frac{\partial}{\partial x_{i}} \left(k \frac{\partial T}{\partial x_{i}} - C_{p} \rho \overline{u_{i} T} \right). \tag{3.12}$$

Methods of determination of the dynamic viscosity and thermal conductivity of pure gases and mixtures of pure gases are presented in section 3.1.

Equations (3.10), (3.11), and (3.12) do not represent a closed system for the determination of the mean velocity U_i , the mean pressure P, and the mean temperature T, since there are six additional unknowns contained within the Reynolds stress tensor which has its origin in the non-linear, advective term of the Navier-Stokes equations. In section 3.2 several models for the Reynoldsstress are presented, and their use is discussed in relation to the present work.

3.1. Gas properties

In the present work the calculation of the viscosity of a pure gas is obtained with the following equation

$$\mu_i = \left[26.693 \cdot 10^{-5} \left(MT\right)^{1/2}\right] / \left(\sigma^2 \Omega\right),$$
(3.13)

where μ_i is the viscosity of the pure gas i, in kg · m⁻¹ · s⁻¹, M is the molecular weight of the gas (in g/mol), T is the absolut temperature (in K), σ is the Lennard-Jones collision diameter (in \mathring{A}), and Ω is the intermolecular force parameter or collision integral which is a function of the dimensionaless temperature factor kT/ϵ , where k is Boltzmann's constant, and ϵ is the minimum

of the potential energy of interaction between two like molecules as they approach each other. The theoretical background and experimental validation of this formula can be found in the book by Bird *et al.* (2002).

A simple semiempirical method of accounting for the energy exchange in polyatomic gases was developed by Eucken, and is presented in the book by Reid *et al.* (1987). Eucken's equation for thermal conductivity of a polyatomic gas at low density reads

$$k_i = \left(C_p + \frac{5}{4} \frac{R}{M}\right) \mu \tag{3.14}$$

where k_i is the thermal conductivity of the pure gas i, in W · m⁻¹ · K⁻¹. μ is the viscosity defined by equation (3.13). This Eucken formula includes the monatomic expression $k=15R\mu/4M$ as a special case, because $C_p=5R/2M$ for monatomic gases.

3.1.2. Mixtures of pure gases

The calculation of the transport properties of gas mixtures is a complex subject. Thorough reviews on the subject can be found in publications by Copeland (2003) and Monnery *et al.* (1995).

The viscosity of a gas mixture is calculated by the semi-empirical formula, equation (3.15), proposed by Wilke (1950).

$$\mu = \sum_{i=1}^{n} \left[x_i \mu_i / \left(\sum_{j=1}^{n} (x_j \Phi_{ij}) \right) \right], \qquad (3.15)$$

while the thermal conductivity of a gas mixture is given by the formula, see Mason & Saxena (1958),

$$k = \sum_{i=1}^{n} \left[x_i k_i / \left(\sum_{j=1}^{n} (x_j \Phi_{ij}) \right) \right], \qquad (3.16)$$

In the two formulae 3.15 and 3.16 the dimensionless quantities Φ_{ij} are:

$$\Phi_{ij} = \frac{1}{8} \left(1 + \frac{M_i}{M_j} \right)^{-1/2} \left[1 + \left(\frac{\mu_i}{\mu_j} \right)^{1/2} \left(\frac{M_j}{M_i} \right)^{1/4} \right]^2, \tag{3.17}$$

where x_i is the mole fraction of the component i, μ_i is the viscosity of the pure component i at the system temperature and pressure. The Φ_{ij} are functions related to the molecular weights and viscosities of each pure component in the mixture. The previous set of formulae is valid only for non polar gases. For the calculation of the transport properties of polar gases please refer to the work by Copeland (2003).

In this thesis, mixtures of only hydrogen and nitrogen were considered. Following of Faura *et al.* (1998), the thermal capacity C_p of mixtures of hydrogen and nitrogen is calculated from the relation

$$C_p = X_{H_2} \times C_{p_{H_2}} + (1 - X_{H_2}) \times C_{p_{N_2}},$$
 (3.18)

where $C_{p_{H_2}}$ is the thermal capacity of pure hydrogen, while $C_{p_{N_2}}$ is the thermal capacity of pure nitrogen.

3.2. Turbulence modeling

In this thesis, two kinds of turbulence models were used. These two models are presented and discussed in detail in the following sections.

The Reynolds stress, $-\overline{u_i u_j}$, is modelled using the Shear Stress Transport (SST) model proposed by Menter (1993). In this model, additional transport equations are solved for the turbulent kinetic energy, k, and the turbulence frequency, ω .

The SST model is a further advancement of the baseline (BSL) k- ω model by Menter (1993). The BSL model is identical to the k- ω model of Wilcox (1988) for the inner region of a boundary layer, up to $y^+ = 11.02$, and gradually changes to the standard k- ϵ model in the outer wake region. The addition of a limiter on the value of the turbulent viscosity ν_t gives the SST model. The structure of the model is outlined in the following and for a more detailed discussion the reader is referred to the original paper by Menter (1993) and the one by Vieser et al. (2001).

In order to be able to perform the computations with one set of equation, the k- ϵ model is first transformed into a k- ω formulation, presented in equations 3.19 and 3.20.

$$\frac{\partial \rho k}{\partial t} + \frac{\partial \rho U_j k}{\partial x_j} = \tau_{ij} \frac{\partial \rho U_i}{\partial x_j} - \beta^* \rho \omega k + \frac{\partial}{\partial x_j} \left((\mu + \sigma_k \mu_t) \frac{\partial k}{\partial x_j} \right)$$
(3.19)

$$\frac{\partial \rho \omega}{\partial t} + \frac{\partial \rho U_j \omega}{\partial x_j} = \frac{\gamma}{\nu_t} \tau_{ij} \frac{\partial U_i}{\partial x_j} - \beta \rho \omega^2 + \frac{\partial}{\partial x_j} \left((\mu + \sigma_\omega \mu_t) \frac{\partial \omega}{\partial x_j} \right)
+ 2 (1 - F_1) \rho \sigma_{\omega 2} \frac{1}{\omega} \frac{\partial k}{\partial x_j} \frac{\partial \omega}{\partial x_j}.$$
(3.20)

where μ_t is the eddy viscosity defined by equation 3.24. The function F_1 is defined as

$$F_1 = \tanh\left(A_1^4\right) \tag{3.21}$$

with

$$A_1 = \min\left(\max\left(\frac{\sqrt{k}}{\beta^*\omega y}, \frac{500\nu}{y^2\omega}\right), \frac{4\rho\sigma_{\omega_2}k}{CD_{k\omega}y^2}\right), \tag{3.22}$$

where y is the distance to the nearest solid wall and $CD_{k\omega}$ is the cross-diffusion term of equation 3.20

$$CD_{k\omega} = \max\left(2\rho\sigma_{\omega_2}\frac{1}{\omega}\frac{\partial k}{\partial x_j}\frac{\partial \omega}{\partial x_j}, 1.0e^{-10}\right),$$
 (3.23)

The eddy-viscosity is defined as

$$\mu_t = \rho \frac{a_1 k}{\max(a_1 \omega; SF_2)},\tag{3.24}$$

where $a_1 = 0.31$ and $S = \sqrt{S_{ij}S_{ij}}$ is the absolute value of the strain rate $S_{ij} = \frac{1}{2} \left(\frac{\partial u_i}{\partial x_j} + \frac{\partial u_j}{\partial x_i} \right)$. Note that Menter (1993) proposed to use the absolute value of the vorticity, Ω . F_2 is given by

$$F_2 = \tanh(A_2^2), \tag{3.25}$$

with

$$A_2 = \max\left(2\frac{\sqrt{k}}{\beta^*\omega y}, \frac{500\nu}{y^2\omega}\right),\tag{3.26}$$

All the coefficients in the above equations are functions of F_1 according to

$$\phi = F_1 \phi_1 + (1 - F_1)\phi_2, \tag{3.27}$$

where ϕ_1 and ϕ_2 stand for the coefficients of k- ω and k- ϵ . The first set of constants (SST - inner) consists of $\sigma_{k1}=0.5,\ \sigma_{\omega 1}=0.5,\ \beta_1=0.0750,\ \beta^*=0.09,\ \kappa=0.41,\ \gamma_1=\beta_1/\beta^*-\sigma_{\omega 1}\kappa^2/\sqrt{\beta^*}.$ The second set of constants (SST - outer) consists of $\sigma_{k2}=1.0,\ \sigma_{\omega 2}=0.0828,\ \beta_2=0.0828,\ \beta^*=0.09,\ \kappa=0.41,\ \gamma_2=\beta_2/\beta^*-\sigma_{\omega 2}\kappa^2/\sqrt{\beta^*}.$

The turbulent stress tensor $\tau_{ij} = -\overline{u_j u_i}$ is

$$\tau_{ij} = \frac{\mu_t}{\rho} \left(\frac{\partial u_i}{\partial x_j} + \frac{\partial u_j}{\partial x_i} - \frac{2}{3} \frac{\partial u_k}{\partial x_k} \delta_{ij} \right). \tag{3.28}$$

The SST turbulence model outlined above has been used in many industrial and academic investigations. Data about validation of the model for aerodynamic applications can be found in Menter (1993), Bardina *et al.* (1997), and Menter (1994).

Automatic wall treatment as described in Vieser et al. (2001) and ANSYS (2004) is used for treatment of solid walls. That gives a relation between wall shear stress and the value of the velocity component parallel to the wall at the nearest wall mesh node. The method is based on an interpolation between the formulation valid for the viscous sublayer and logarithmic wall functions depending on the size of the grid and the character of the flow near the wall.

As the ω equation provides analytical solutions, both for the sublayer and the logarithmic region, a blending function depending on the dimensionless wall distance $y^+ = \rho y \sqrt{\tau_w/\rho}/\mu$ can be defined, τ_w being the wall shear stress and y the wall distance. The solutions for ω in the linear, ω_{vis} , and logarithmic, ω_{log} , near-wall regions are

$$\omega_{vis} = \frac{6\mu}{\rho 0.075y^2},\tag{3.29}$$

$$\omega_{log} = \frac{1}{0.3\kappa} \frac{u_{\tau}}{y}, \tag{3.30}$$

which can be reformulated in terms of y^+ and a smooth blending function as

$$\omega(y^{+}) = \left(\omega_{vis}^{2}(y^{+}) + \omega_{log}^{2}(y^{+})\right)^{0.5}, \tag{3.31}$$

can be defined. It is of importance to notice that no explicit reference to the limiting $y^+ = 11.02$ is made. A similar formulation is used for the velocity profile near the wall, as stated in equations 3.32, 3.33, and 3.34.

$$u_{\tau}^{vis} = \frac{U_t}{y^+}, \tag{3.32}$$

$$u_{\tau}^{log} = \frac{U_t}{\frac{1}{\kappa}ln(y^+) + C}, \tag{3.33}$$

$$u_{\tau} = \left[\left(u_{\tau}^{vis} \right)^4 + \left(u_{\tau}^{log} \right)^4 \right]^{0.25}$$
 (3.34)

where C = 5.0. This formulation gives the relation between the velocity at the first node near the wall, U_t , and the wall shear stress. For the k-equation 3.19 a zero flux boundary condition is applied, as this is correct both for the low Reynolds number and the logarithmic limit.

3.2.2. Differential Reynolds Stress model

The RSM model used in the study performed by Macchion $et\ al.\ (2004a)$ is the commonly used LLR QI, developed by Launder & Rodi (1975), where the transport of the Reynolds stresses is expressed as

$$\frac{\partial}{\partial t}(\rho \overline{u_i u_j}) + \frac{\partial}{\partial x_k}(U_k \rho \overline{u_i u_j}) = P_{ij} + \phi_{ij} + D_{ij} - \frac{2}{3}\delta_{ij}\rho\epsilon. \tag{3.35}$$

where P_{ij} is the stress production term and ϕ_{ij} is the pressure-strain correlation. The third term is the diffusion term and the last term is the dissipation term. The constant σ_k has a value of 0.82. Except in the vicinity of the wall boundaries, k is determined from the Reynolds stresses as $k = \frac{1}{2}\overline{u_i}\overline{u_i}$. Terms that require additional modelling are the pressure-strain correlation, ϕ_{ij} , and the dissipation term, ϵ . The scalar dissipation rate ϵ -equation is defined similarly to the k- ϵ model. The pressure-strain term can be written as the summation of two different terms

$$\phi_{ij} = \phi_{ij}^1 + \phi_{ij}^2 \tag{3.36}$$

where ϕ_{ij}^1 is the return-to-isotropy term and ϕ_{ij}^2 , the rapid pressure-strain term. An additional wall reflection term, $\phi_{ij,\omega}$, could be included. It redistributes the Reynolds stresses near the wall to dampen the terms perpendicular to the wall and to enhance the terms parallel to the wall. Preliminary results indicated that it did not produce marked difference in the solutions and therefore it was excluded. ϕ_{ij}^1 and ϕ_{ij}^2 are formulated as

$$\phi_{ij}^1 = -C_1 \rho \frac{\epsilon}{k} \left[\overline{u_i u_j} - \frac{2}{3} \delta_{ij} k \right], \qquad (3.37)$$

where C_1 is 1.8, and

$$\phi_{ij}^2 = -C_2 \left[(P_{ij} - C_{ij}) - \frac{1}{3} \delta_{ij} (P_{kk} - C_{kk}) \right], \tag{3.38}$$

where C_2 is 0.60. C_{ij} is the convection term defined as the second term on the left hand side of equation (3.35).

3.3. Solution methodology

To solve the above equations, a commercially available code, CFX 5 was used in its successive versions, CFX 5.5, 5.6, and finally 5.7. The equations are discretized on an unstructured, non-staggered mesh by a finite volume formulation. The continuity equation is approximated using a second order central difference approximation to the first order derivative in velocity, modified by a fourth order derivative in pressure based on the Rhie-Chow interpolation method. The advection scheme used in this study is the high resolution scheme, a form of total variation diminishing scheme, proposed by Barth & Jesperson (1989). If the cell-centred value of a variable is ϕ , then the face value ϕ_f can be expressed as

$$\phi_f = \phi + \beta \nabla \phi \cdot \delta \vec{s} \tag{3.39}$$

where $\nabla \phi$ is the gradient of ϕ in the upstream cell, $\delta \vec{s}$ is the displacement vector from the upstream cell to the face centroid and β is the blending factor. When β is 1, the scheme becomes a second-order upwind scheme. In the high resolution scheme, β is set to be as close to 1 as possible, without causing numerical problems.

A coupled solver is used to solve the set of discretized equations. Details of the numerical method used in the code CFX-5 can be found in ANSYS (2004). To take full advantage of the turbulence modeling that was used in this thesis, most computations were performed with very fine meshes near walls. In most cases, y^+ values were below 2.

CHAPTER 4

Summary of results

In this chapter a summary of the results directly applicable to gas quenching furnace design is presented. In addition to the work summarized here, the large eddy simulation methodology has been evaluated as a tool for investigation of turbulence fluctuations. The result of that study is only discussed in the work by Macchion (2005) (Paper 7).

The factors influencing the heat transfer around a bluff body are discussed starting with the difficulty of modeling flows around blunt bodies in section 4.1. Section 4.2 presents some features of the axial flow and heat transfer around a cylinder placed in a periodic stack. In section 4.3 the influence of gas mixture composition is presented. These sections summarize the work presented in Macchion & Zahrai (2004) (Paper 3) and Macchion et al. (2004b) (Paper 5).

The hydrodynamics and heat transfer within the VUTK gas quenching furnace follows in section 4.4. In section 4.4.1 the numerical method presented in chapter 3 is validated, the case being the empty VUTK furnace. Section 4.4.2 presents summarized results of the work presented in the texts by Macchion $et\ al.\ (2004c)\ (Paper\ 1)$ and Macchion $et\ al.\ (2005b)\ (Paper\ 2)$, where the flow and heat transfer around and over two types of charges, one made of plates, the other of cylinders, were computed. A focus on the influence of the dimensions of the quenching chamber is performed in sectionch:quenchcorr, parts of the results presented here being taken from Macchion $et\ al.\ (2005a)\ (Paper\ 6)$.

Sections 4.6 and 4.7 focus on the influence of the design of the entrance to the quenching chamber on flow uniformity. Detailed studies of such topic can be found in the studies performed by Macchion *et al.* (2004a) (Paper 4) and Macchion *et al.* (2004c) (Paper 1).

4.1. Heat transfer around a cylinder in axial homogeneous flow

The prediction of the flow around a bluff body has triggered a large interest in the past years. Lots of research has been performed on models describing with accuracy the complex flows arising around objects like cars, buses, and trains. In gas quenching, most metal pieces to quench are bluff bodies, giving rise to massive flow separations, See e.g. Igarashi (1981), Roshko (1955), Roshko (1993), and Koenig & Roshko (1985).

4.1. HEAT TRANSFER AROUND A CYLINDER IN AXIAL HOMOGENEOUS FLOW

In this work the focus has been on the use of eddy-viscosity models, relatively more simple than Reynolds stress models. The choice of the eddy-viscosity models was done both to save computational resources, and to ensure that one obtains a converged result in a reasonable time. This ensures that the method validated in the present section can be used in an industrial context.

In the following, numerical predictions of the flow and heat transfer around a cylinder in axial flow are discussed. The test cylinder dimensions are $D=0.15~\mathrm{m},\,L=0.3~\mathrm{m}.$

Table 4.1. Mesh sizes.

Mesh	Size	$U_1 [\mathrm{m/s}]$	T[K]
1	1225800	-3.3	260
2	2500000	-3.3	272
3	3580000	-3.2	275

Table 2 presents the mesh specifications. Two criteria were considered, the first being the streamwise velocity U_1 at a point 50 mm behind the test cylinder, on the axis of the cylinder, the second being the temperature at the separation point on the cylinder. Figure 4.1 presents the mesh topology that was used to obtain the final result.

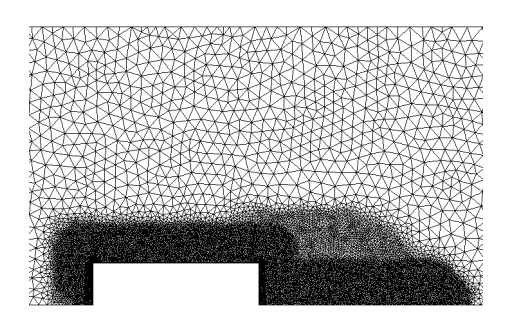


FIGURE 4.1. Mesh.

Figure 4.2 shows the comparison between experimental heat transfer data and the heat transfer coefficient calculated using the SST model presented in chapter 3. The mesh used to perform this calculation is the mesh number 3 in table 2. s denotes a dimensionless coordinate along the surface of the cylinder. s = 2y/D on the front surface of the cylinder, s = 2x/D on the lateral surface of the cylinder, and s = 2y/D on the back surface of the cylinder. Thus $0 \le s \le 1.0$ corresponds to a point on the front surface, $1.0 \le s \le 5.0$ corresponds to a point on the lateral surface, $5.0 \le s \le 6.0$ corresponds to a point on the back surface. The agreement is generally good, as qualitatively similar trends are observed

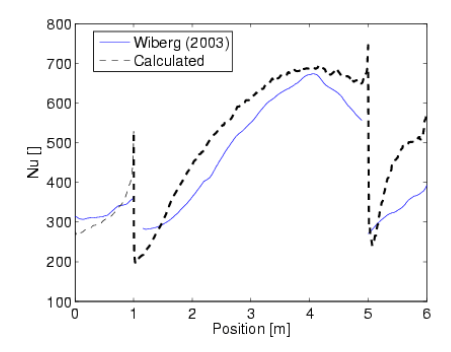


FIGURE 4.2. Comparison between experimental and calculated heat transfer data over the test cylinder (D = 0.15 m, L = 0.3 m).

in both experimental and computational results. Between s=0 and s=1, the agreement is good, with an apparent overprediction of the Nusselt number towards the edge of the cylinder at s=1. However it is generally agreed, see Wiberg & Lior (2003), that measurements obtained by the thermochromic liquid crystal technique are not reliable close to edges. Between s=1 and s=5, the numerical result agrees qualitatively well with the experimental data. The length of the separation bubble is correctly predicted. The largest error in the calculation of the Nusselt number is about 13 %. Large deviations are observed on the back face, between s=5 and s=6. These deviations come from the fact that the cylinder used during the experiment was mounted on a rod, about 20 mm in diameter, attached to the back face of the cylinder. The cables feeding the heating elements on the cylinder went through this rod.

Figure 4.3 shows the axisymmetric recirculation bubble formed around the cylinder after separation at the leading edge. This picture is representative of the flow field observed in every one of the cases that were computed in the present paper. It has been shown experimentally, see Wiberg & Lior (2003), that the length of the separation bubble does not depend on the Reynolds number.

4.2. Influence of quenching basket on heat transfer

Macchion & Zahrai (2004) (Paper 3) made a summary of the results presented by Macchion $et\ al.\ (2004c)$ (Paper 1) and Macchion $et\ al.\ (2005b)$ (Paper 2). They investigated also the influence of the geometry of the quenching basket on the uniformity of the heat transfer over a cylinder placed in a different periodic pattern, plotted on figure 4.4.

The geometries of the quenching baskets that were tested are plotted on figure 4.5. In figure 4.5(a) the cylinders stand alone in the quenching chamber, with no basket to keep them in place. In figure 4.5(b), the basket is made of bars, that are about two to three mm thick, and that are currently used

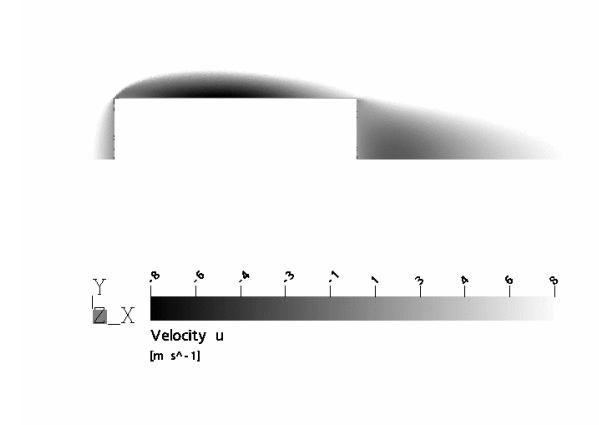


FIGURE 4.3. Separation bubble over the test cylinder (D = 0.15 m, L = 0.3 m).

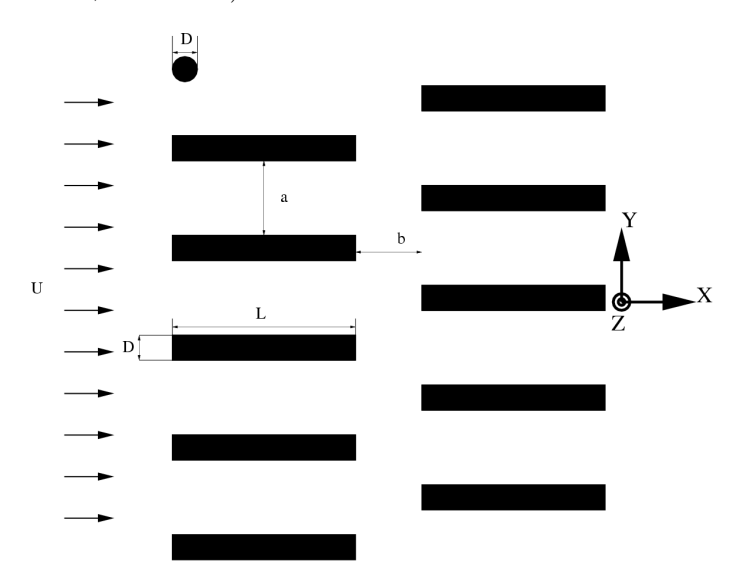


FIGURE 4.4. A bank of warm cylinders (D=28 mm, L=110 mm) in axial flow

in industrial gas quenching processes. In figure 4.5(c) the basket is made of plates, three mm thick, that form a quadratic shape around the cylinder to be cooled. In figure 4.5(d), the basket is made of round plates, three mm thick, that espouse the shape of the metal piece to be quenched.

Figures 4.6 and 4.7 present the heat transfer contours over the lateral surface of a cylinder placed in the four different configurations described on

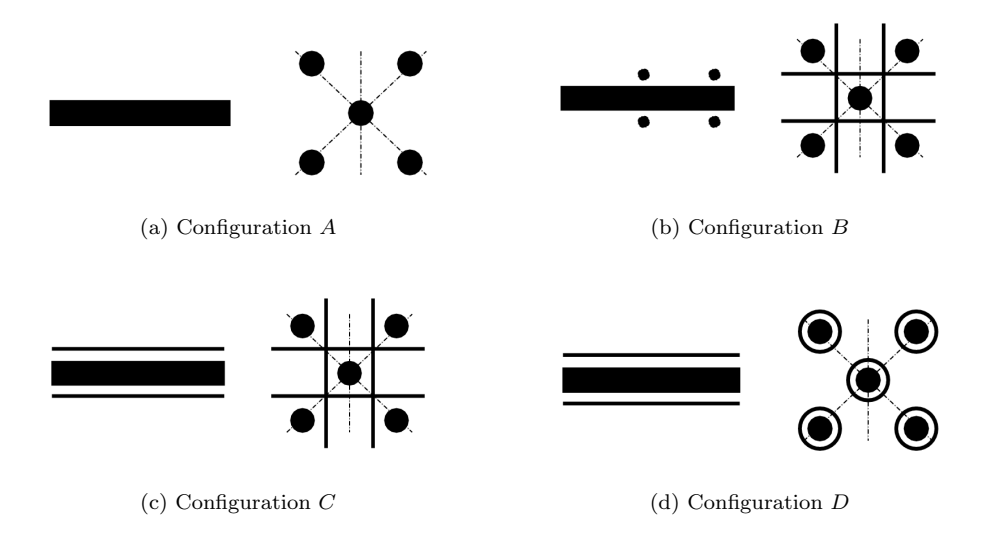


FIGURE 4.5. Four quenching basket configurations are delineated. Fig. 4.5(a): No basket, the cylinders stand alone in the quenching chamber. Fig.4.5(b): Basket made of bars, currently used in industrial gas quenching processes. Fig. 4.5(c): Basket made of thick walls. Fig. 4.5(d): Basket made of round walls.

figure 4.5. Figure 4.6(a) shows the heat transfer contours over the cylinder placed in a stack of cylinders without any holding device. The heat transfer distribution appears to be varying close to the leading edge of the cylinder, between x = 0 and x = 40. Beyond x = 40, the heat transfer distribution is uniform.

Figure 4.5(b) shows the heat transfer contours over the cylinder in the Ipsen basket, made of cylindrical bars. The heat transfer distribution appears to be varying close to the leading edge of the cylinder, between x=0 and x=40, mimicking the distribution obtained in the first configuration. At x=50 and x=100, increase in heat transfer by 25 % can be observed. These locations correspond to the position of the holding bars.

Figures 4.7(a) and 4.7(b) present the heat transfer contours over the cylinder in baskets made of straight and round plates of 3 mm in thickness, respectively. The heat transfer appears to be homogeneous over the whole length of the cylinder.

The results obtained when using the configuration presented in figure 4.5(c) have been experimentally verified during testing performed at Ipsen International GmbH. An adaptation of such a configuration has been tested and was

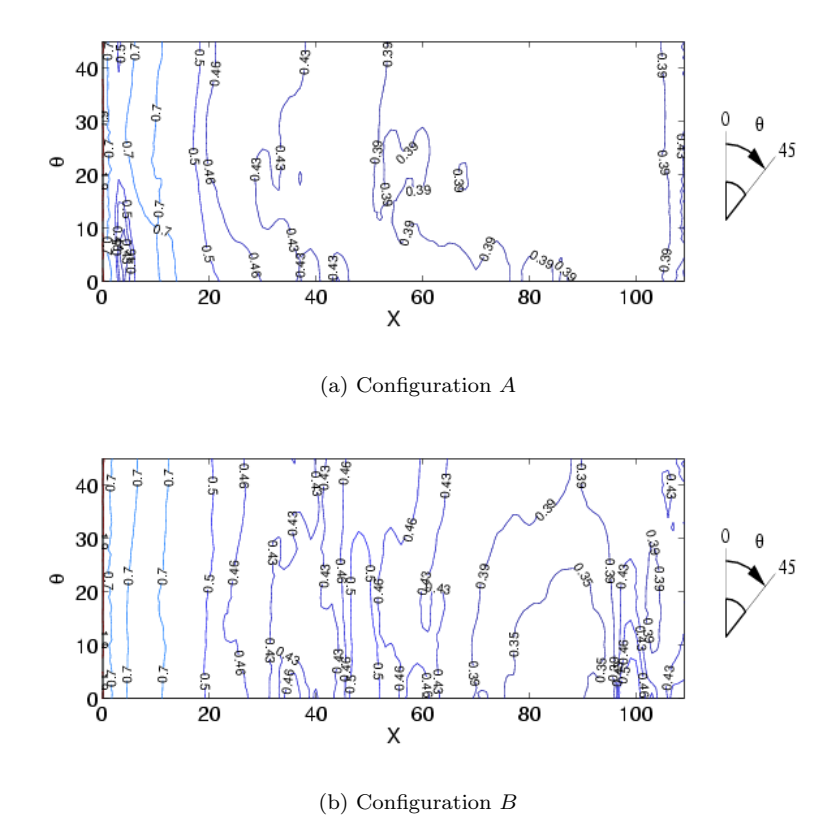


FIGURE 4.6. Heat transfer distributions over the lateral surface of the test cylinder in the configurations A and B.

found to lead to much improved results when it comes to heat transfer uniformity and final product quality.

4.3. The influence of gas mixture composition

In this section a short overview of the influence of gas mixture composition on heat transfer over a cylinder is presented. A more detailed perspective, including the influence of gas mixture composition on heat transfer uniformity, is available in the work by Macchion $et\ al.\ (2004b)\ (Paper\ 5).$

Figure 4.8 shows the variation of mean heat transfer coefficient as a function of the hydrogen content, X_{H_2} , on the surface facing the incoming flow and the lateral surface of the cylinder. On the front surface the mean heat transfer coefficient $\overline{h_w}$ grows nearly linearly with the hydrogen content X_{H_2} for $X_{H_2} \leq 0.6$. For $X_{H_2} \geq 0.6$ the evolution departs from a linear behaviour and the increase in the heat transfer coefficient is less. The maximum mean heat transfer coefficient is found for pure hydrogen, which is in contradiction with

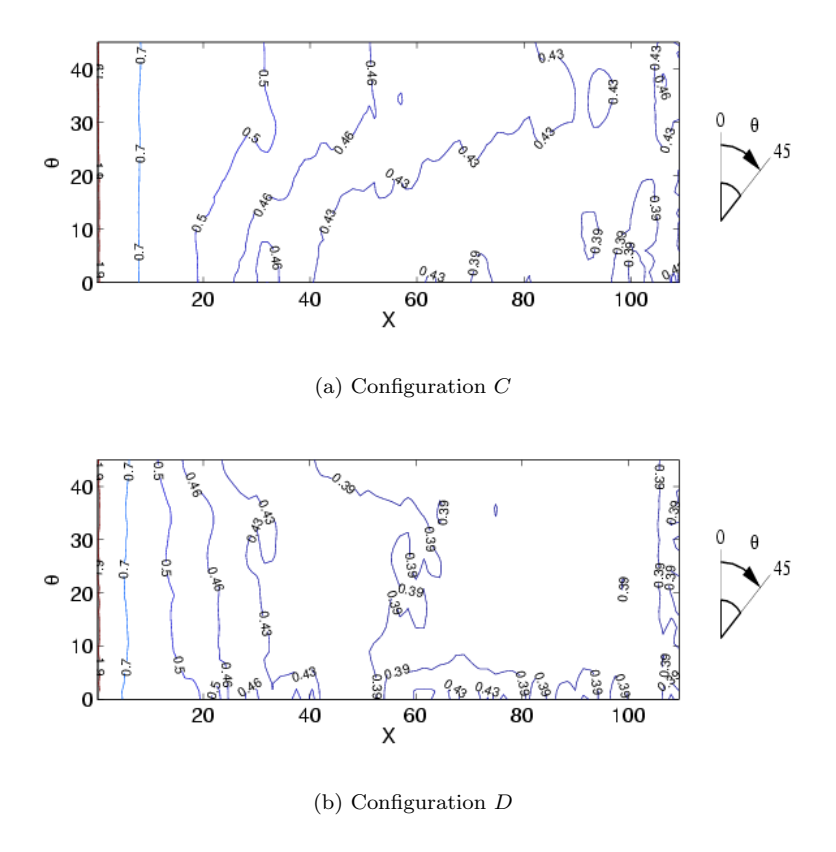


FIGURE 4.7. Heat transfer distributions over the lateral surface of the test cylinder in the configurations C and D.

the measurement data of Laumen Laumen et al. (1997). On the lateral surface the mean heat transfer coefficient $\overline{h_w}$ grows with the hydrogen content X_{H_2} until $X_{H_2} = 0.8$. For $X_{H_2} \geq 0.8$ $\overline{h_w}$ decreases until it reaches the mean heat transfer coefficient got for pure hydrogen, $\overline{h_{w_{N_2}}} = 130$ W· m⁻²· K⁻¹. An interesting point is that all mixtures with $X_{H_2} \geq 0.46$ lead to higher mean heat transfer coefficients than for pure hydrogen.

4.4. Gas quenching furnace

In this section the hydrodynamics and heat transfer within the VUTK gas quenching furnace are presented. A coordinate system is defined in the following way. The axis Y is along the major axis and the axis Z along the minor axis of the furnace presented in figure 2.2. The main direction of the flow from the entrance box to the exit trap in denoted by X. Consequently, the plates are parallel to XZ plane with the center of the middle one coinciding with the origin of the coordinate system , i.e. $x=0,\,y=0,$ and z=0. The cylinders

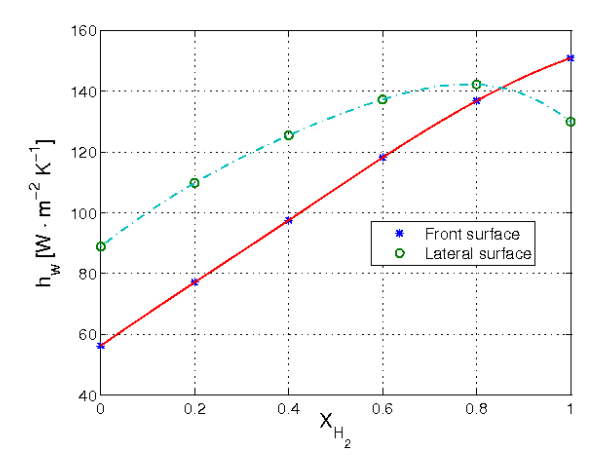


FIGURE 4.8. Variation of the mean heat transfer coefficient over the front and lateral surfaces of the cylinder, as a function of gas mixture composition.

are placed at three different YZ planes with three cylinders in the direction of Y and five cylinders in the direction of Z. The center of the cylinder in the middle of the second plane coincides with the origin of the coordinate system. In the first case the empty furnace is modeled as a reference for comparison with experimental data. In the second case, the furnace is charged with 7 plates of dimensions $500 \times 500 \times 70$ mm, half of which included in the computational domain. These plates are referred to as $P_{(-3)}$ to $P_{(+3)}$; $P_{(0)}$ will be the plate situated in the middle of the chamber. The third case consists of the VUTK furnace charged with 45 cylinders, of length 150 mm and diameter 120 mm, where only 15 complete cylinders and 15 half-cylinders are included in the simulation. The cylinders are referred to by a C with three indices denoting the location of the cylinder. As an example, $C_{(0)(0)(0)}$ will be the one in the middle of the charge, $C_{(-1)(0)(0)}$ will be the one in the middle of the plane near the entrance and $C_{(+1)(+2)(+1)}$ will be the cylinder located at the lower corner of the charge.

4.4.1. Validation of the computational model

Two series of velocity measurements were performed in the empty furnace presented in section 2.2, using a Pitot tube. The first set of measurements was done just below the entrance trap, the second was performed at x=0.1 m. Comparison of the results presented in figure 4.9 with this set of measurements shows that the average velocity across the core of the chamber is correctly predicted by the numerical model, the relative error being within 10 % of the experimental results. Large deviations observed at x=-0.3 and z=0.35 could be caused by eddies generated in that region as will be discussed below.

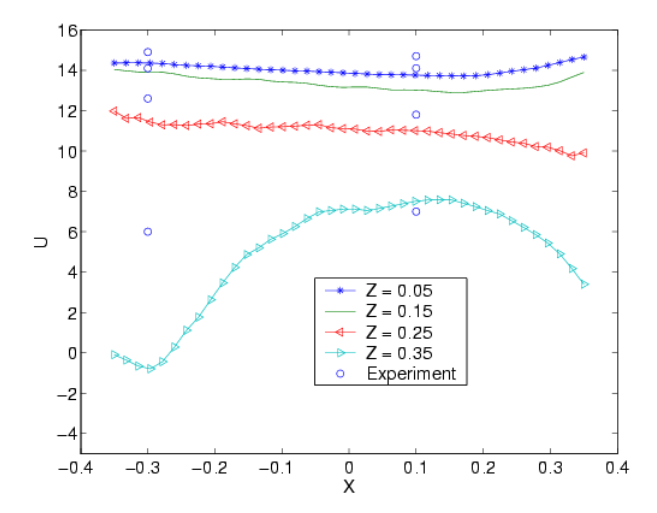


FIGURE 4.9. Comparison between experimental and computational results for the streamwise velocity U along a plane XZ at Y=0.0 - Empty furnace

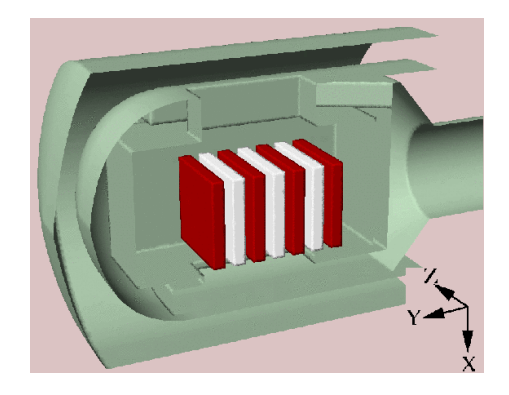
4.4.2. Multi-body charges

Macchion et al. (2004c) (Paper 1) and Macchion et al. (2005b) (Paper 2) investigated the influence of multi-body charges on the performance of the VUTK furnace. Two different configurations are considered as examples of the charge. The first configuration consists of 7 plates of dimensions $500 \times 500 \times 70$ mm and in the second configuration, the VUTK furnace is charged with 45 cylinders, of length 150 mm and diameter 120 mm placed with their symmetry axis parallel to the main flow. These cylinders are at three horizontal planes with 5×3 cylinders at each plane. See figure 4.10.

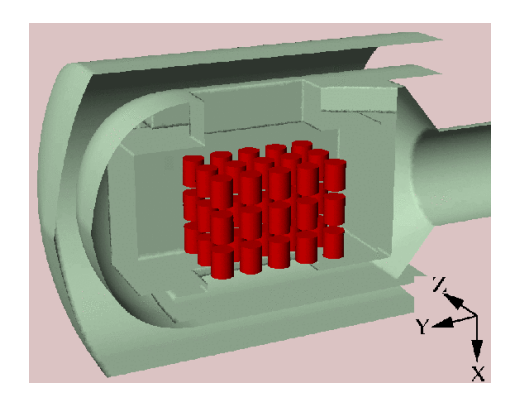
The charge in the above configurations is assumed to be quenched in nitrogen at the reference pressure of 10 bar at a volume flow of 42000 m³/h. This volume flow results in an inlet velocity of 3.35 m/s. The Reynolds number was of the order of $2 \cdot 10^6$.

Streamwise velocity contours at the inlet of the chamber are presented for all three cases in figure 4.11. As can be seen here, the flow is at acceptable levels of homogenity in the three cases. A measure of uniformity is the dimensionless standard deviation, which reads 0.2, 0.09, and 0.1 respectively for the empty furnace, the case with plates, and the case with cylinders.

Figure 4.12 presents the flow pattern in the symmetry plane (z=0). In an empty chamber, the flow between the inlet and the outlet in the center of the chamber is close to uniform. This region is surrounded by two dead volumes created by the sudden expansion and sudden contraction of the chamber, where the gas is in relatively slow recirculating motion and forms two large circulating



(a) Furnace charged with plates



(b) Furnace charged with cylinders

FIGURE 4.10. Furnace geometry with the different charges used for investigation of charge effects

patterns. These circulating flows could make the velocity measurements more difficult and cause the deviations observed above.

With the same total flow of mass, the presence of the charge reduces the flow cross section area, resulting in increase of the velocity. The blockage also forces the gas out from the basket into the side regions at a high velocity, resulting in creation of stronger eddies and a more complex flow pattern, as seen in figures 4.12(a), 4.12(b) and 4.12(c). As noted in this figure, qualitatively similar behavior is observed in the case of the furnace charged with cylinders.

Figure 4.13 presents some streamwise velocity and heat transfer coefficient profiles over six neighbouring cylinders in the case charged with cylinders. The study by Macchion $et\ al.\ (2005b)$ (Paper 2) gives a presentation of similar data

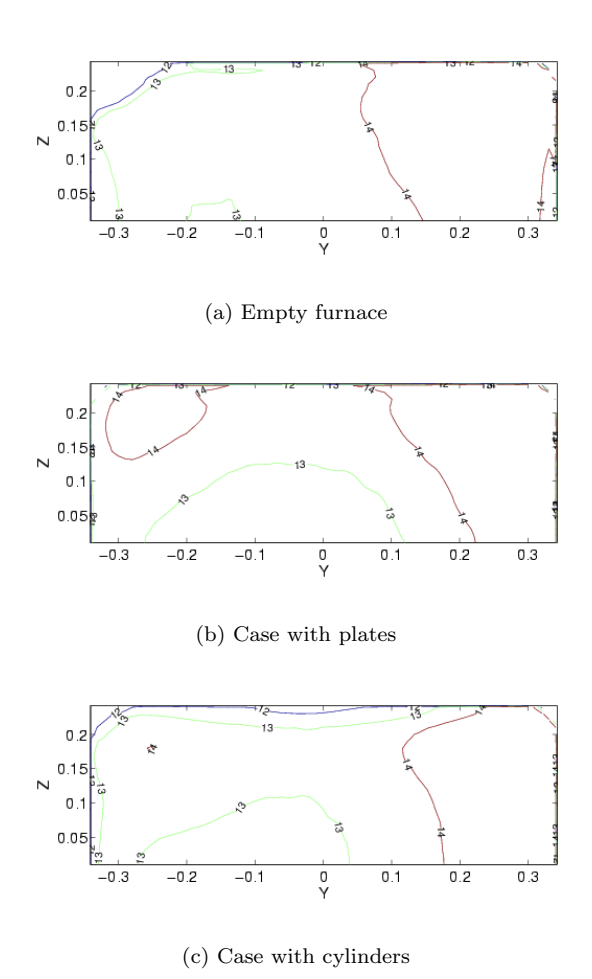
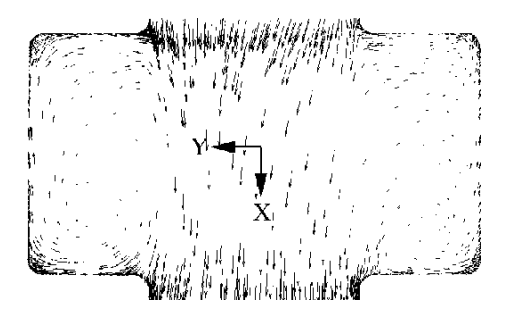
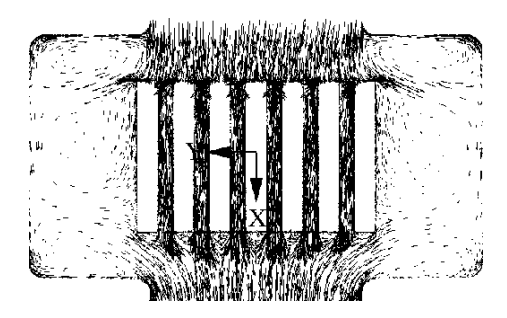


FIGURE 4.11. Streamwise velocity contours at the exit of the entrance box (X = -0.45 m)

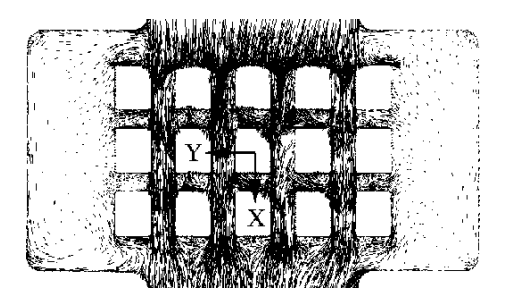
for the case with plates. The profiles are based on curves perpendicular to the symmetry plane at z=0. In figure 4.13(a) the velocity profiles appear flatter on the four last cylinders, $C_{(0)(0)(0)}$, $C_{(+1)(0)(0)}$, $C_{(+1)(0)(+1)}$, and $C_{(0)(0)(+1)}$ than on the two first cylinders, $C_{(-1)(0)(0)}$ and $C_{(-1)(0)(+1)}$. The velocity profiles on the first set of cylinders at x=-0.28, x=-0.21, and x=-0.14 are not symmetric. They show that the flow is entirely separated on the cylinder $C_{(-1)(0)(0)}$ (Z=0.06) while the flow is not separated on cylinder $C_{(-1)(0)(+1)}$. It is important to stress that these observations are not valid for the whole circumference of the cylinders. Figure 4.13(b) shows the heat transfer coefficient to be higher on the first row of cylinders, $C_{(-1)(0)(0)}$ and $C_{(-1)(0)(+1)}$ than on the two following rows, where the heat transfer coefficient displays about the same mean and



(a) Empty furnace



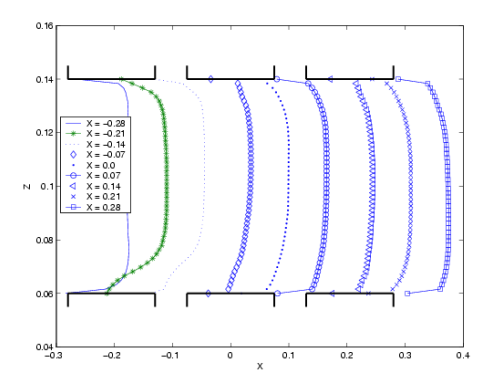
(b) Case with plates



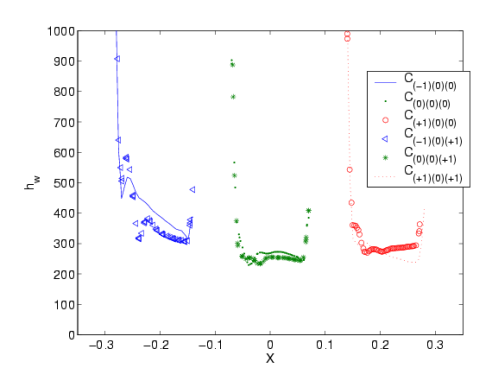
(c) Case with cylinders

FIGURE 4.12. Transverse velocity vectors through the working chamber $% \left(1\right) =\left(1\right) \left(1\right) +\left(1\right) \left(1\right) \left(1\right) +\left(1\right) \left(1\right) \left($

distribution. This result has been discussed with the industrial partners of the project, and the agreement is good with what has been observed experimentally.



(a) Velocity profiles between cylinders $C_{(-1)(0)(0)}$ and $C_{(-1)(0)(+1)}$, $C_{(0)(0)(0)}$ and $C_{(0)(0)(+1)}$, $C_{(+1)(0)(0)}$ and $C_{(+1)(0)(+1)}$,



(b) Heat transfer coefficient distribution on cylinders $C_{(-1)(0)(0)}$ and $C_{(-1)(0)(+1)}$, $C_{(0)(0)(0)}$ and $C_{(0)(0)(+1)}$, $C_{(+1)(0)(0)}$ and $C_{(+1)(0)(+1)}$

FIGURE 4.13. Relation between velocity profile and heat transfer coefficient evolution in the uniform flow region - Case with cylinders $\frac{1}{2}$

4.5. Chamber geometrical characteristics and chamber performance

Macchion et al. (2005a) (Paper 6) shows that the influence of the quenching chamber proportions both on the mean heat transfer and the heat transfer uniformity, can be defined through relations of the type

4.5. CHAMBER GEOMETRICAL CHARACTERISTICS AND CHAMBER PERFORMANCE

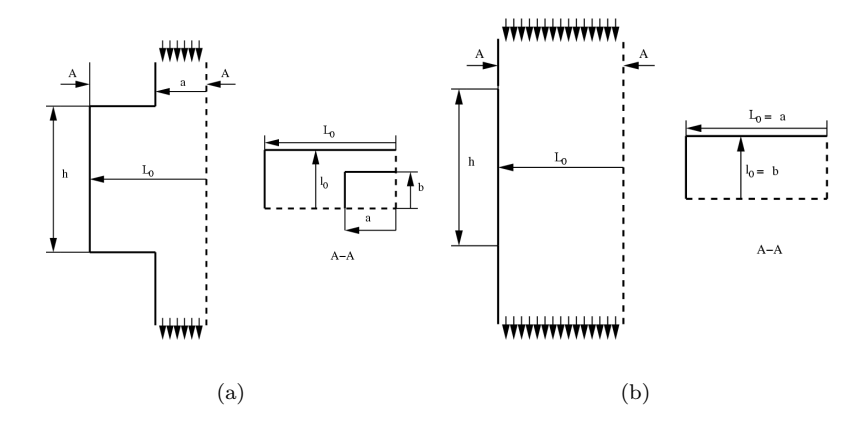


FIGURE 4.14. Variations on the VUTK geometry presented in chapter 2.

$$\overline{Nu} = f(R, Re_D) \cdot \overline{Nu_0}, \tag{4.1}$$

$$Nu_{rms} = g(R, Re_D) \cdot Nu_{rms}^0, \tag{4.2}$$

where f and g are functions depending only on the distance R to the axis in the streamwise direction X, $\overline{Nu_0}$ is the Nusselt number of a single body in axial flow, Re_D is the characteristic Reynolds number of the flow within the charge, while Nu_{rms}^0 is the normalized standard deviation of the heat transfer over a body in axial flow.

Figure 4.14(a) presents the general shape of the type of quenching chamber considered here. The quenching chamber, i.e. the chamber where the quenching process takes place, has a parallelepipedic shape with two rectangular openings opposing each other. The one through which the gas enters the chamber is usually called the upstream opening and the other is called the downstream opening. The openings have length a and width b, while the chamber has length L_0 , width l_0 , and height b. The dimensions are given in the work by Macchion et al. (2005a) (Paper 6). Figure 4.14(b) is a particular case of the geometry presented in figure 4.14(a), where the opening length a is equal to L_0 , while the opening width b is equal to b0. The different designs are characterized by the aspect ratio

$$AR = \frac{\sqrt{a^2 + b^2}}{L_0^2 + l_0^2} \tag{4.3}$$

which is the ratio between the diagonal of the openings, and the diagonal of the chamber. When this ratio is 0, the chamber is closed, when the ratio is 1.0, the openings have the same length and width than the chamber. The last particular case is the one presented in figure 4.14(b).

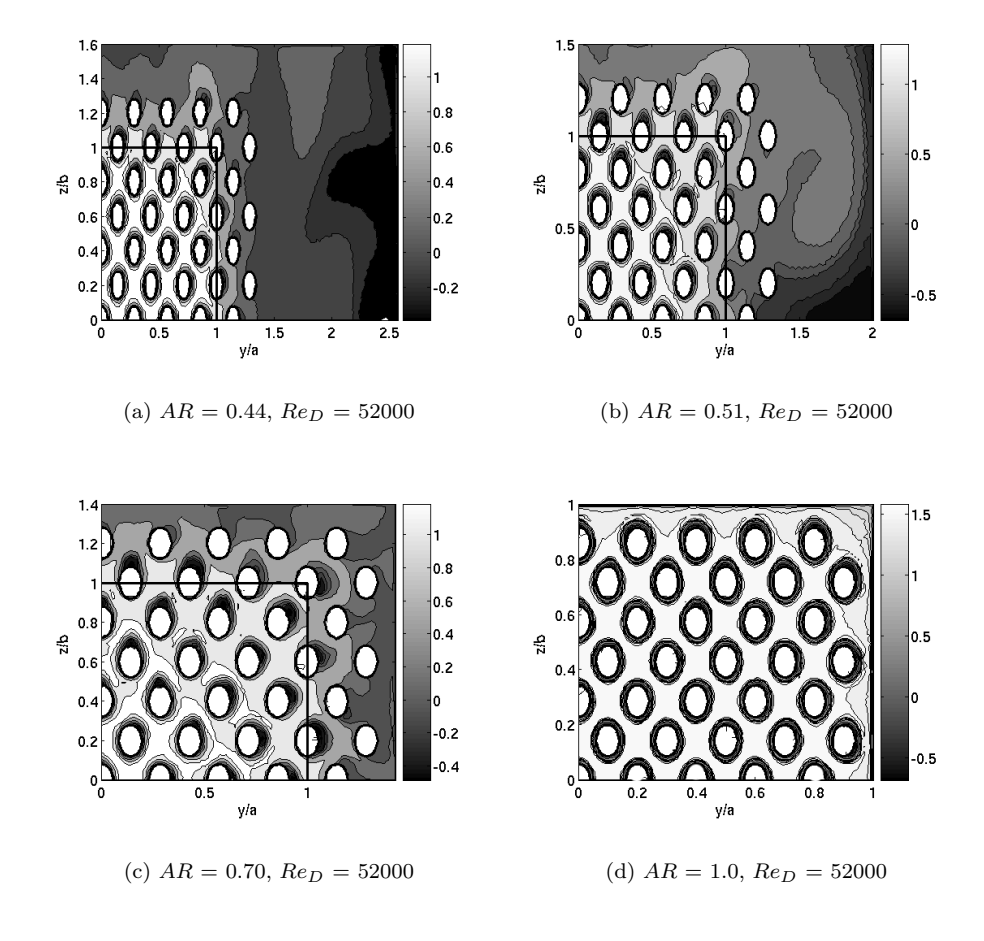


FIGURE 4.15. Streamwise velocity contours on the middle plane (x = 0) in the charged chambers $(Re_D = 52000)$.

The influence of the quenching chamber proportions on the homogeneity of the velocity field can be estimated from figure 4.15.

Figure 4.15 shows contours of streamwise velocity on the plane located at x=0, perpendicular to the main stream and to the axis X, in the four charged chambers at $Re_D=52000$. In figures 4.15(a), 4.15(b), and 4.15(c), the thick black line is the projected position of the upstream opening through which the flow enters the quenching chamber.

Figures 4.15(a) and 4.15(b) present the streamwise velocity contours in the chambers with AR = 0.44 and AR = 0.51. As discussed by Macchion *et al.* (2004c) (Paper 1), a large recirculating motion can be observed, in both cases, in the region of the chamber where there is no cylinders to be quenched. In the case AR = 0.44, the intensity of the recirculating motion, measured by the

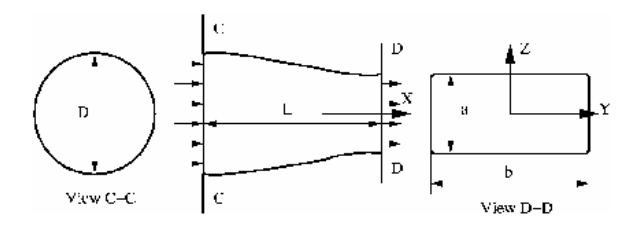


FIGURE 4.16. Example of the geometry of the circular-to-rectangular transition ducts that have been tested. Here AL = L/D = 1.5, AR = a/b = 2.0.

minimum velocity obtained in the dead zone, is -0.3. In the case AR = 0.44 the intensity of the recirculating motion is -0.6.

Figures 4.15(c) and 4.15(d) present the streamwise velocity contours in the chambers with AR=0.7 and AR=1.0. Large differences in the velocity contours can be observed. Contrary to what is reported by Macchion *et al.* (2004c), no large recirculating motion is visible. On figure 4.15(c) areas of negative velocities, that is to say separation bubbles, are visible on the sides of the cylinders looking away from the axis X. Such observation is not made on figure 4.15(d). The velocity contours appear to be more uniform on figure 4.15(d) than on figure 4.15(c).

4.6. Flow uniformity and duct geometry.

The computational sensitivity analysis performed in Macchion $et\ al.\ (2004a)$ (Paper 4) aimed at investigating the influence of the design of circular-to-rectangular transition ducts, see figure 4.16, on the flow uniformity upstream of the charge, in furnaces of the type manufactured by Ipsen International GmbH for research purposes, today installed in Bremen, Germany. Influence of length was tested by varying the length aspect ratio AL = L/D between 0.7 and 1.5. Influence of AL was shown by computing the flow in ducts whose exit AR = a/b was varied from 1.0 to 4.0 (square shape to rather flat rectangle). Here L is the length of the transition duct, while D is the inlet diameter. The parameters a and b are the semi-major and semi-minor axis, respectively. Comparison of flows in an expanding-contracting duct and a constant cross-sectional area duct was performed. Influence of pressure (1, 6, and 20 bar) and Reynolds number in the range (1.3)10⁵ $< Re < (7.8)10^5$ (10, 20, 30 and 60 m s⁻¹ at the inlet plane) were studied.

Flows in several transition ducts have been studied. The transition ducts' cross sectional shapes were designed by using a sequence of superelliptic cross

sections,

$$\left(\frac{y}{a}\right)^{\eta} + \left(\frac{z}{b}\right)^{\eta} = 1\tag{4.4}$$

As written earlier, a and b are respectively the semi-major axis and semi-minor axis of the superellipse, η is the exponent. Circles with a=b and $\eta=2$, and rectangles, with $\eta\to\infty$, are included in this family of curves. The inlet diameter of each transition duct was D=0.204 m (dimensions of the experimental duct), as the duct used in the work by Davis & Gessner (1992) was taken as a reference for most computations.

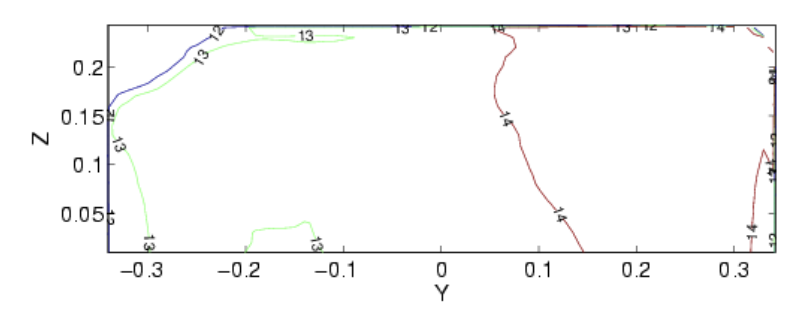


Figure 4.17.

The maximum height and width of the duct cross section were represented by cubic functions which were chosen to achieve continuity of the second derivative at the end points of the ducts. These functions give the values of a and b, parameters of the superellipse. The exponent of the superellipse was calculated from an implicit function relating the quantities a, b, and η to the area A of the superellipse

$$A = \frac{\Gamma(1/\eta)^2}{\Gamma(1/\eta)} (2/\eta) \cdot (4ab) \tag{4.5}$$

where $\Gamma\left(\cdot\right)$ denotes the gamma function. As seen in equation , the relationship between a,b, and η determines also the radius at the corners of the rectangular cross section by setting the value of η . Following Davis & Gessner (1992), it was chosen to have $\eta=10$ for all geometries. This value corresponds to a radius of r=0.015 m at the corners of the rectangular cross-section. We also note that the magnitude of r has some influence on the flow distribution and pressure drop, with larger r tending to improve uniformity and reduce pressure drop, but this has not been examined in this thesis.

For AL < 1.0, flow distortion at the exit plane and pressure drop are increased respectively by 33 % and 83 % as AR decreases. Exit AR > 1.5 lead to linearly increasing distortion and pressure drops, the pressure drop being K=0.02 at AR=1.5, and K=0.11 at AR=4.0. A diverging-contracting duct has proven to lead to less distortion, while it did not influence the pressure drop. Increasing the inlet pressure from 1 to 20 bar led to a decrease in flow

distortion by 11 % at the duct exit planes. At atmospheric pressure, increasing the Reynolds number from $(1.3)10^5$ to $(7.8)10^5$ increased distortion by 8 %. For a detailed account of the results obtained in this study, refer to Macchion *et al.* (2004a) (Paper 4).

4.7. Flow uniformity upstream of the charge.

Streamwise velocity contours at the inlet of the chamber are presented for the empty VUTK furnace in figure 4.17. As can be seen here, the flow is at acceptable levels of homogenity. The measure of uniformity presented in section 2.5 reads 0.2. This value, compared with the sensitivity analysis performed by Macchion et al. (2004a) (Paper 4) and briefly presented in section 4.6, shows that the present design of the VUTK furnace leads to flow uniformity upstream of the charge close to the best achievable uniformity.

CHAPTER 5

Concluding remarks

Numerical predictions of the flow and heat transfer over bluff bodies and within gas quenching chambers have been performed, using commercial codes. Good agreement between experimental data and computational results has been obtained.

The main focus has been set on one particular type of single-chamber furnace, the VUTK furnace, commercialized by Ipsen International GmbH, one of the industry partners of this project. It has been found that some of the design choices that were made during the conception of the VUTK led to non-homogeneous flow distribution, and thus non-homogeneous heat transfer within the load area.

These observations led to suggestions for improvements, which after discussion with the industrial partners, Linde Gas and Ipsen International GmbH, have led to the following set of recommendations regarding the future design of single-chamber furnaces:

- 1. The upstream and downstream doors should be larger than the dimensions of the basket containing the metal pieces to quench.
- 2. The distance between the quenching chamber walls and the quenching basket should be kept to a minimum, determined by the constraints placed on the heating apparatus located in the chamber.

On the basis of these two simple recommendations, the start of a new design project has been initiated.

Concerning the arrangement of the metal pieces within the chamber, the following set of recommendations could be given:

- 1. The use of dummies on the first row of the quenching basket arrangement would seem to be beneficial, at least from the point of view of the uniformity of the mean heat transfer through the charge.
- 2. As demonstrated by the work performed by Macchion $et\ al.\ (2005a)$, the arrangement of the metal pieces and the dimensions of the basket should be such that the distance between objects and quenching chamber walls be the same.

Further studies were performed on the influence of the quenching basket holding the metal pieces to be quenched within the quenching chamber. It was found that the geometry of the quenching basket has a strong influence on the heat transfer distribution over the metal piece to be quenched. It is suggested that the quenching basket may be used as an enhancement device.

This study has mainly focused on the influence of the furnace design parameters on the performance of the quenching process. As discussed in chapter 2, gas quenching of low-alloy steels necessitates the use of large over-pressures, typically 20 bar, which lead to the need for expensive safety equipment. Future research in this branch should focus on obtaining high cooling rates at atmospheric pressure. Examples of such methods exist for the quenching of irons, where water sprays are used. The study by de Oliveira et al. (2002) has shown that such method leads to controlled homogeneous quenching of pieces of complex shapes. The challenge would be to develop spray quenching using non-corrosive coolants for steels instead of irons.

Another avenue of research would consist in developing cooling apparatus for continuous processes, like the weld seam of steel tubes, which necessitates high cooling rates over short times after annealing of the tubes. Studies by other researchers, like the work performed by Su et~al.~(2003), have shown that heat transfer coefficients of the order of 850 W·m $^{-2}$ s $^{-1}$ can be obtained at atmospheric pressure with jets of air charged with liquid nitrogen droplets. For comparison, such high heat transfer rates can be obtained with nitrogen gas at 20 bar over-pressure.

Acknowledgments

This work was financed by the VINNOVA competence centre, Faxénlaboratoriet, with the two main industrial partners of this project, Ipsen International GmbH, and Linde Gas.

I would like to thank my supervisor Said Zahrai for all the valuable feedback, help, and friendship, he has given me from the moment when he took over the supervision of my work.

I would also like to thank Jan Bouwman at Ipsen International GmbH, today retired, but who has helped me in many ways.

Efforts of Anders Åström, at Linde Gas, resulted in a tight collaboration between Faxénlaboratoriet and the industrial partners giving me a real inspriration for carrying out the work in this thesis. I want to thank him for that and all discussions and help I could have during the course of my work.

I would like to address many thanks to Michael Vynnycky, for the interesting discussions on the value of research, the trips to the forest, and his friendship. I have learnt a lot from you for which I am very grateful.

I want to thank all my colleagues at the department for providing a good working atmosphere and interesting discussions, in particular Jordan Ko, Ola Danielsson, and Mattias Jansson. I would like to address special thanks to Niklas Mellgren, for his help and friendship during the long hours spent over weekends at the office, especially these last six months.

Professor Fritz Bark is acknowledged for his interest in my work and his leading role within Faxénlaboratoriet. I am also grateful to Professor Arthur Rizzi for his support and advice during the early stages of my doctoral studies.

I would like to address special thanks to Ingunn Wester, Viviana Wallin, and Pär Ekstrand for their professional attitude and hard work at the department.

I would also like to thank my parents for their support.

Last but not least. Boel, thank you for your love and your patience.

Bibliography

- Anon 1978a Gas turbine engine inlet flow distortion guidelines. In Society of Automotive Engineers, SAE ARP 1420.
- Anon 1978b Inlet total pressure distortion considerations for gas turbine engine. In Society of Automotive Engineers, SAE AIR 1419.
- ANSYS 2004 ANSYS CFX Reference Manual. cfx-support-uk@ansys.com.
- ARTS, T., LAMBERT DE ROUVROIT, M. & UTHERFORD, A. W. 1990 Aero-thermal investigation of a highly loaded transonic linear turbine guide vane cascade. *Tech. Rep.*. von Karman Institute for Fluid Dynamics, Belgium, technival Note 174.
- BARDINA, J. E., HUANG, P. G. & COAKLEY, T. J. 1997 Turbulence modeling validation. *AIAA Paper 97-2121 28th* AIAA Fluid Dynamics Conference, 4th AIAA Shear Flow Control Conference.
- Barth, T. & Jesperson, D. 1989 The design and application of upwind schemes on unstructured meshes. AIAA Paper 89-0366.
- BIRD, R. B., STEWART, E. W. & LIGHTFOOT, E. N. 2002 Transport phenomena. New York: Wiley & Sons.
- BLESS, F. & EDENHOFER, B. 1997 Advances in increasing the quenching speed of single-chamber vacuum furnaces with high-pressure gas-quench systems. *Heat Treatment of Metals* 1997.4, 89–91.
- Butler, R. J., Byerley, A. R., Vantreuren, K. & Baughn, J. W. 2001 The effect of turbulence intensity and length scale on low-pressure turbine blade aerodynamics. *International Journal of Heat and Fluid Flow* 22, 123–133.
- COPELAND, D. A. 2003 New approximate formulas for viscosity and thermal conductivity of dilute gas mixtures. AIAA Journal 41 (3), 525–537.
- DAVIS, D. O. & GESSNER, F. B. 1992 Experimental investigation of turbulent flow through a circular-to-rectangular transition duct. *AIAA Journal* **30**, 367–375.
- FAURA, F., CAMPO, A. & ZAMORA, B. 1998 A mixture of pure gases that produce maximum heat transfer characteristics for quenching. *Journal of Materials Engineering and Performance* 7 (3), 420–424.
- HANCOCK, P. E. & Bradshaw, P. 1983 The effect of free-stream turbulence on turbulent boundary layer flow and heat transfer. *Journal of Fluids Engineering* **105**, 284.
- HUNT, J. C. R. 1973 A theory of turbulent flow round two-dimensional bluff bodies. Journal of Fluid Mechanics 61, 625, part 4.

- IGARASHI, T. 1981 Characteristics of the flow around two circular cylinders arranged in tandem (1st report). Bulletin of JSME 24 (188), 1858–1865.
- Koenig, K. & Roshko, A. 1985 An experimental study of geometrical effects on the drag and flow field of two bluff bodies separated by a gap. *Journal of Fluid Mechanics* **156**, 167–204.
- Laumen, C., Midea, S. J., Lubben, T., Hoffmann, F. & Mayr, P. 1997 Measured heat transfer coefficients by using hydrogen as quenchant in comparison with helium and nitrogen. In *ASM Heat Treatment Conference*. Indianapolis.
- Launder, B.E. Reece, G. & Rodi, W. 1975 Progress in the development of a reynolds-stress turbulence closure. *Journal of Fluid Mechanics* **68** (3), 537 566.
- LEFANTZI, S. & KNIGHT, D. D. 2002 Austomated design optimization of a threedimensional s-shaped subsonic diffuser. *Journal of Propulsion and Power* 18 (4).
- MACCHION, O. 2005 Large eddy simulation of flow and heat transfer over a cylinder in axial flow. $to\ be\ submitted$.
- MACCHION, O., LIOR, N. & RIZZI, A. 2004a Computational study of velocity distribution and pressure drop for designing some gas quench chamber and furnace ducts. *Journal of Materials Processing Technology* In Press.
- MACCHION, O. & ZAHRAI, S. 2004 Cfd for the design of gas quenching furnaces. 17th Nordic Seminar on Computational Mechanics .
- MACCHION, O., ZAHRAI, S. & ASTROM, A. 2004b On the influence of gas mixture composition on gas quenching uniformity and mean. To be published.
- MACCHION, O., ZAHRAI, S., ASTROM, A. & RINK, M. 2005a Heat transfer correlation in gas quenching chamber. to be submitted.
- Macchion, O., Zahrai, S. & Bouwman, J. 2004c On hydrodynamics within gas quenching furnace. Submitted to the Journal of Materials Processing Technology
- MACCHION, O., ZAHRAI, S. & BOUWMAN, J. 2005b Thermal effects within gas quenching furnace. Submitted to the Journal of Materials Processing Technology, short version published in IASME Transactions 1(2), January 2005, p. 137-142.
- MASON, E. A. & SAXENA, S. C. 1958 Thermal conductivity of mixtures. *Physics of Fluids* 1, 361–369.
- MENTER, F. 1993 Zonal two equation k- ω turbulence models for aerodynamic flows. AIAA Paper 93-2906 24th Fluid Dynamics Conference (Orlando).
- MENTER, F. R. 1994 Two-equation eddy-viscosity turbulence models for engineering applications. *AIAA Journal* **32** (8), 1598–1605.
- Monnery, W. D., Svrcek, W. Y. & Mehrotra, A. K. 1995 Viscosity: a critical review of practical predictive and correlative methods. *The Canadian Journal of Chemical Engineering* 73, 3–40.
- DE OLIVEIRA, M., WARD, J., GARWOOD, D. R. & WALLIS, R. A. 2002 Quenching of aerospace forgings from high temperatures using air-assisted, atomized water sprays. *Journal of Materials Engineering and Performance* 11 (1), 80–85.
- REID, R. C., PRAUSNITZ, J. M. & POLING, B. E. 1987 The properties of gases and liquids, 4th edn. New-York: McGraw-Hill.
- ROSHKO, A. 1955 On the wake and drag of bluff bodies. *Journal of the aeronautical sciences* (2), 124–132.

- Roshko, A. 1993 Perspectives on bluff body aerodynamics. *Journal of Wind Engineering and Industrial Aerodynamics* 49, 79–100.
- Su, L., Chang, S., Yeh, C. & Hsu, Y. 2003 Heat transfer of impinging air and liquid nitrogen mist jet onto superheated flat surface. *International Journal of Heat and Mass Transfer* 46, 4845–4862.
- Tennekes, H. & Lumley, J. L. 1972 A first course in turbulence. Cambridge: MIT Press, iSBN 0262200198.
- Thuvander, A., Melander, A., Lind, M., Lior, N. & Bark, F. 1998 Prediction of convective heat transfer coefficients and examination of their effects on distortion of tubes quenched by gas cooling. In 4th ASM Heat Treatment and Surface Eng. Conf. in Europe. Florence, Italy.
- TOTTEN, G. E., BATES, C. E. & CLINTON, N. A. 1993 Quenchants and Quenching Technology. ASM International, iSBN 0-87170-448-X.
- TROELL, E. & SEGERBERG, S. 1995 Cooling in nitrogen and helium under high pressure. *Tech. Rep.* IVF-Skrift 95845. The Swedish Institute of Production Engineering Research (IVF), Gothenburg.
- Van Fossen, G. J. & Ching, C. Y. 1994 Measurements of the influence of integral length scale on stagnation region heat transfer. Fifth Int. Sym. on Transport Phenomena and Dynamics of Rotating Machinery (ISROMAC-5) Paper No. TP-16.
- Van Fossen, G. J. & Simoneau, R. J. 1994 Stagnation region heat transfer: The influence of turbulence parameters, reynolds number, and body shape. *AIAA/ASME Thermophysics and Heat Transfer Conference* Colorado Springs, Colorado.
- Van Fossen, G. J., Simoneau, R. J. & Ching, C. Y. 1995 Influence of turbulence parameters, reynolds number, and body shape on stagnation-region heat transfer. ASME J. Heat TRansfer 117, 597–603.
- VIESER, W., ESCH, T. & MENTER, F. 2001 Heat transfer predictions using advanced two-equation turbulence models. *Tech. Rep.* CFX-VAL10/0602. CFX.
- Wiberg, R. & Lior, N. 2003 Convection heat transfer coefficients for axial flow gas quenching of a cylinder. In *Proceedings of the Fourth International Conference on Quenching and the Control of Distortion*.
- WILCOX, D. C. 1988 Reassessment of the scale-determining equation for advanced turbulence models. AIAA Journal 26 (11), 1299–1310.
- WILKE, C. R. 1950 A viscosity equation for gas mixtures. *Journal of Chemical Physics* 18, 517–519.
- ZUKAUSKAS, A. A. 1987 Convective heat transfer in cross flow. In *Handbook of Single-Phase Convective Heat Transfer* (ed. S. Kakac, R. K. Shah & W. Aung), chap. 6. New York: Wiley.